Experience-dependent predictions of feedforward and contextual information in mouse visual cortex

Koen Seignette[1,2*], Leander de Kraker[1], Paolo Papale[3], Lucy S. Petro[4,5], Barbara Hobo[6], Jorrit S. Montijn[7], Matthew W. Self[3], Matthew E. Larkum[2], Pieter R. Roelfsema[3,8,9,10], Lars Muckli[4,5] & Christiaan N. Levelt[1,11,**]

1. Department of Molecular Visual Plasticity, Netherlands Institute for Neuroscience, Amsterdam, Netherlands
2. Department of Biology, Humboldt Universität zu Berlin, Berlin, Germany
3. Department of Vision & Cognition, Netherlands Institute for Neuroscience, Amsterdam, Netherlands
4. Centre for Cognitive Neuroimaging, School of Psychology and Neuroscience, College of Medical, Veterinary and Life Sciences, University of Glasgow, Glasgow, UK
5. Imaging Centre for Excellence (ICE), College of Medical, Veterinary and Life Sciences, University of Glasgow, UK
6. Department of Neuroregeneration, Netherlands Institute for Neuroscience, Amsterdam, Netherlands
7. Department of Cortical Structure & Function, Netherlands Institute for Neuroscience, Amsterdam, Netherlands
8. Laboratory of Visual Brain Therapy, Sorbonne Université, Institut National de la Santé et de la Recherche Médicale, Centre National de la Recherche Scientifique, Institut de la Vision, Paris, France
9. Department of Integrative Neurophysiology, Centre for Neurogenomics and Cognitive Research, VU University, Amsterdam, Netherlands
10. Department of Psychiatry, Academic Medical Center, University of Amsterdam, Amsterdam, Netherlands
11. Department of Molecular and Cellular Neurobiology, Center for Neurogenomics and Cognitive Research, VU University Amsterdam, Amsterdam, Netherlands

*Current affiliation

**Correspondence: (c.levelt@nin.knaw.nl)

ABSTRACT

Neurons in primary visual cortex are driven by feedforward visual inputs and top-down contextual inputs. The nature of this contextual information is difficult to study, as responses to feedforward and top-down inputs overlap in time and are difficult to disentangle experimentally. To address this issue, we measured responses to natural images and partially occluded versions of these images in the visual cortex of mice. Assessing neuronal responses before and after familiarizing mice with the non-occluded images allowed us to study experience-dependent and stimulus-specific contextual responses in pyramidal cells (PyCs) in cortical layers 2/3 and 5 in the absence of feedforward input. Surprisingly, in the same retinotopic region of cortex, we found that separate populations of PyCs in layer 2/3 responded to occluded and non-occluded images. Responses of PyCs selective for occluded images were strengthened upon familiarization and decoding analysis revealed they contained image-specific information, suggesting that they signaled the absence of predicted visual stimuli. Responses of PyCs selective for non-occluded scenes were weaker for familiarized images but stronger for unfamiliar images, suggesting that these neurons signaled the presence of unpredicted visual stimuli. Layer 5 also contained PyCs preferring either feedforward or contextual inputs, but their responses were more complex and strengthening of responses to occluded images required task engagement. The results show that visual experience decreases the activity of neurons responding to known feedforward inputs but increases the activity of neurons responding to contextual inputs tied to expected stimuli.

INTRODUCTION

Neurons in primary visual cortex (V1) respond to visual stimuli present in confined regions of the visual field known as their classical receptive fields (cRFs). These inputs are provided by feedforward signals from the retina, via the dorsolateral geniculate nucleus (dLGN) of the thalamus. However, neurons also receive contextual information from regions that are far from the cRF, originating from higher-order cortical regions, provided through lateral and top-down connections[1–4]. The nature of this contextual information is difficult to study because responses to feedforward and top-down inputs overlap in time and are difficult to disentangle experimentally[5].

To explore this issue, experiments have been conducted involving the presentation of partially occluded visual stimuli, thus eliminating feedforward inputs to a retinotopic region of V1. Human fMRI studies[6–11] and multiunit recordings in non-human primates[12] have shown that partially occluded natural scenes even drive responses of V1 neurons with cRFs in a non-stimulated quarter-field. These responses are image specific, because a classifier trained on the responses to occluded image regions can be used to decode the identity of the non-occluded parts and generalizes to responses elicited by the corresponding non-occluded image. This cross-classification from occluded but inferred information (top-down) to non-occluded information (bottom-up) indicates that these different streams share information. It further suggests that neurons responding to the non-occluded images can also be activated by the visual context alone. However, this form of contextual modulation has not been investigated at the level of individual neurons, but only with multiunit recordings in monkeys[12]. These recordings revealed that the responses to occluded information are stimulus specific and delayed by 40 ms compared to the non-occluded, stimulus-driven response, consistent with the notion that the occluded image information is processed by top-down projections. The V1 activity elicited by occluded image regions has also been investigated using fMRI in humans, implicitly averaging across tens of thousands neurons in the voxels[7,9]. A study that compared activity across the layers with 7T fMRI indicated that the occluded image information was predominantly processed in super-granular layers of V1[6].

It is useful to consider responses to partially occluded images in the context of predictive coding. According to this theory, the brain constructs an internal model of the environment based on prior experiences[13–17]. The internal model is continuously compared with incoming sensory information, and the brain strives to minimize disparities between the model and the visual input by computing errors in the predictions and utilizing these to update the model. Prediction errors can be negative, signaling the absence of a predicted stimulus, or positive, signaling the unpredicted appearance of a stimulus[16]. Within this predictive coding framework, responses to occluded visual scenes may either represent predictions about the missing content or negative prediction errors signaling the absence of this content. Responses to the non-occluded images would represent positive prediction errors, signaling the unexpected appearance of new visual stimuli.

To understand whether responses to occluded and non-occluded images align with predictive coding, it is crucial to assess the role of prior visual experience. Predictive coding holds that images that are more familiar and thus more predictable are expected to evoke weaker prediction errors than unpredictable novel images. In contrast, when familiar images are occluded, responses are expected to be increased as predictions and thus prediction errors are stronger. In addition, theories of predictive coding posit that the internal model and positive and negative prediction errors are computed in specialized neuronal populations[16,19]. It is thus important to understand how responses to occluded and non-occluded images are organized at the level of individual cells and how they change with experience.

To address these questions, we presented mice with non-occluded and partially occluded natural images before and after familiarizing them with a subset of the non-occluded images. During image presentation, we measured responses of pyramidal cells (PyCs) in layer 2/3 (L2/3) and layer 5 (L5) using wide-field and two-photon calcium imaging. This approach allowed us to assess how prior visual experience influences the responses of individual PyCs to non-occluded and occluded images. We find that separate populations of PyCs in L2/3 and L5 respond to either feedforward or contextual information and that these responses are influenced by visual experience. Our results support the idea that mouse V1 contains neurons that respond to unpredicted stimuli or absence of predicted stimuli. To our surprise, the nature of these prediction errors did not align

with contemporary models of predictive coding in which error signals reflect the locally computed difference between predicted and actual stimuli[14,16,20].

RESULTS

Studying the impact of visual experience on feedforward and contextual responses

To test the effect of visual experience on neuronal responses to non-occluded and occluded scenes, we trained mice in a simple stimulus detection task. Before and after learning, we recorded calcium signals from PyCs in L2/3 and L5 of primary visual cortex (V1) using wide-field (WF) and two-photon (2P) microscopy, while presenting the mice with six different non-occluded and occluded natural images (Figure 1A-D). The luminance of the occluded area was equal to that of the gray screen during the intertrial interval, so that no change occurred in the cRF of the recorded neurons when the occluded image appeared (Figure 1A).

During behavioral training, we presented mice with only four out of the six images, and only the non-occluded versions of them. Licking in the time window 1-2 s after disappearance of any image resulted in a small water reward. Mice learned to associate the stimuli with a reward, leading to stimulus-locked licking and high hit rates (Figure 1E-F). During the passive imaging sessions before (naive mice) and after (expert mice) training, mice were not performing the task but passively viewed the stimuli. In addition, to test the influence of engagement we recorded responses in one extra 2P session during task performance (during task). Excluding two out of six images from the training paradigm allowed us to compare experience-dependent changes in neuronal responses to familiar (i.e. used for training) and novel (i.e. not used for training) images.

We performed calcium imaging in L2/3 and L5 PyCs in separate groups of mice using the following approach. For L2/3 PyCs, we recorded in TIT2L-GCaMP6f x G35-3-Cre mice, in which Cre is expressed in cortical excitatory neurons[21] (Figure 1B). For L5 PyCs, we recorded in Rbp4-Cre mice[22] mice after a tail vein injection of a Cre-dependent PhP.eB-serotyped[23] AAV GCaMP6f vector, resulting in L5 PyC-specific expression (Figure 1C). We targeted our recordings to the

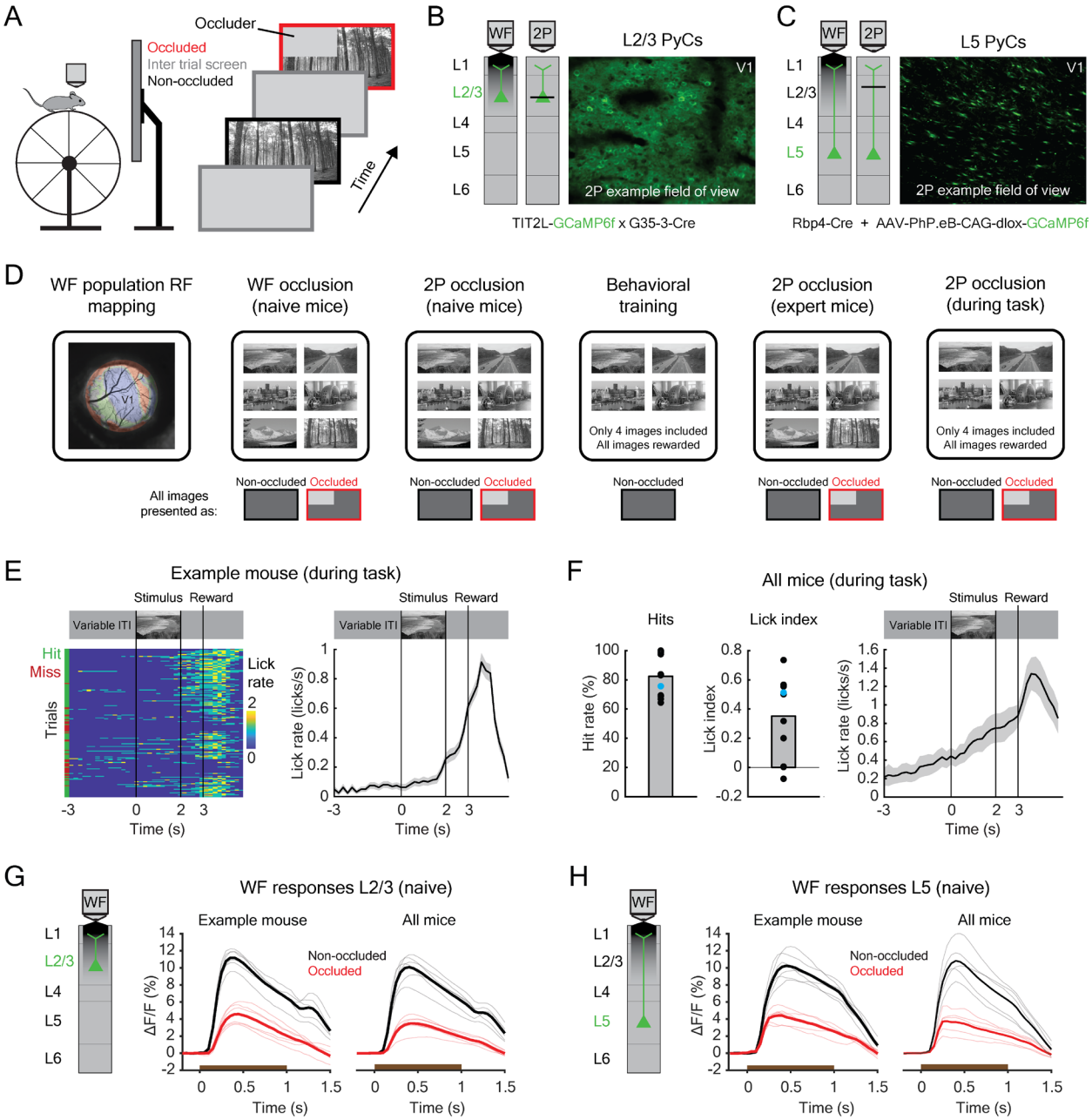

Figure 1. Experimental setup to study plasticity of visual and contextual responses across cell types in mouse V1

A) Schematic of experimental setup. Mice were head-fixed on a running wheel centered in front of a screen displaying non-occluded and occluded natural scenes.

B) Imaging approach showing wide-field (WF) and two-photon (2P) calcium imaging in L2/3 neurons in V1 of TIT2L-GCaMP6f x G35-3 mice.

C) As in B, but for L5 neurons in Rbp4-Cre mice labeled by a tail vein injection of a viral vector encoding cre-dependent GCaMP6f.

D) Schematic of calcium imaging and behavioral training steps. 'Naive' mice were subjected to a WF population RF mapping session followed by retinotopically targeted WF and 2P occlusion experiments. 2P

sessions were performed before (naive) and after (expert) a behavioral training phase to familiarize mice with the natural scenes. For behavioral training we used a subset (4/6) of the images, without occlusion. One additional 2P imaging session with familiar images was performed while the mice were engaged in the task (during task).

E) Schematic of task structure and licking behavior for an example mouse (blue dot in F). Water restricted mice were required to lick in the interval of 1-2 s after disappearance of a non-occluded natural scene to obtain a water reward. Left: lick rate for individual trials. Right: trial-averaged average lick rate.

F) Left: average hit rate for individual mice during the task session. Middle: lick index for individual mice (see Materials and Methods). Right: trial-averaged lick rate (mean ± SEM across mice).

G) Average L2/3 WF responses to non-occluded and occluded visual stimuli for an example mouse (left, thin lines represent individual images, thick line represents mean across images) and all mice (right, thin lines represent individual mice, thick line represents mean across mice).

H) As in G, but for L5.

region of V1 that retinotopically represented the occluded quadrant of the natural scenes. To achieve this, we first used wide-field (WF) calcium imaging to perform a population receptive field (pRF) mapping[24] session immediately followed by the occlusion experiment (Figures 1D and S1). We used the pRF maps to extract WF signals from V1 that represented the occluded quadrant of the scenes (taking a safety margin of 7 visual degrees to minimize bleed-through from neighboring regions). In Rbp4-cre mice, the GCaMP6f signal was derived from L5 PyCs, while in TIT2L-GCaMP6f x G35-3-Cre mice the signal may have derived from PyCs in all layers, but was presumably dominated by L2/3. The non-occluded and occluded scenes elicited diverse yet robust responses in all mice (Figures 1G-H, S1B and S1D). This result confirms that the regions of mouse visual cortex that represent the occluded region of a natural scene, and that therefore receive no feedforward input from the dLGN, are nevertheless activated, just like in humans[7,9] and monkeys[12].

Experience and engagement drive opposite plasticity of responses to non-occluded and occluded images

Although we minimized bleed-through from nearby regions in our WF occlusion data, we wanted to fully exclude the possibility that part of the response to occluded stimuli comes from neighboring non-occluded retinotopic regions. We therefore used two-photon (2P) calcium imaging to record the responses from individual L2/3 or L5 PyCs. In addition, we studied how

these responses depended on visual experience and whether they were layer-dependent by comparing the activity of L2/3 PyC somas and L5 PyC apical dendrites (Figure 1B-C).

Using the WF pRF map, we targeted our 2P imaging to the region of V1 representing the occluder (Figure 2A). We then mapped the cRF location of all recorded neurons using sparse noise stimuli and applied strict criteria to only include neurons in subsequent analyses with high quality cRFs falling on the occluded region and not on the non-occluded image regions (see Materials and Methods and Figure 2B).

We first focused on stimuli repeatedly presented during the training phase (familiar images, Figure 2C-E). For statistical comparisons we used a linear mixed effects model (LMEM), which accounts for dependencies in the data and variance between mice. Visual experience had profound effects on L2/3 PyC responses to non-occluded and occluded stimuli. In naive mice, many neurons responded to occluded stimuli (Figure 2C) although responses to non-occluded stimuli were stronger. Notably, in expert mice, responses to occluded stimuli were strongly increased (Figure 2D-E, LMEM: $P < 0.001$ for all comparisons), an effect that was even more profound during task performance. In contrast, responses to non-occluded stimuli showed the opposite pattern. They decreased in expert mice and mice performing the task (LMEM: $P < 0.001$ for naive versus expert, $P < 0.001$ for naive versus task and $P = 0.999$ for expert versus task).

Plasticity in L5 PyCs showed a different pattern. Responses to non-occluded stimuli also decreased with experience and task engagement (Figures 2F-2J, LMEM: $P < 0.001$ for naive versus expert, $P < 0.001$ for naive versus task and $P < 0.01$ for expert versus task), but in contrast to the situation in L2/3 PyCs, the responses of L5 PyCs to occluded stimuli did not increase significantly (LMEM: $P = 0.881$ for L5 naive versus expert; LMEM interaction effect: $P < 0.001$ for naive versus expert L2/3 compared to naive vs expert L5). It was only when the mice were engaged in the task following learning that L5 PyCs showed an enhanced response to occluded stimuli (Figures 2I-2J, LMEM: $P < 0.001$ for naive versus task and $P < 0.001$ for expert versus task). This suggests that contextual input through visual experience is less effective at strengthening responses in L5 PyCs, and requires task engagement.

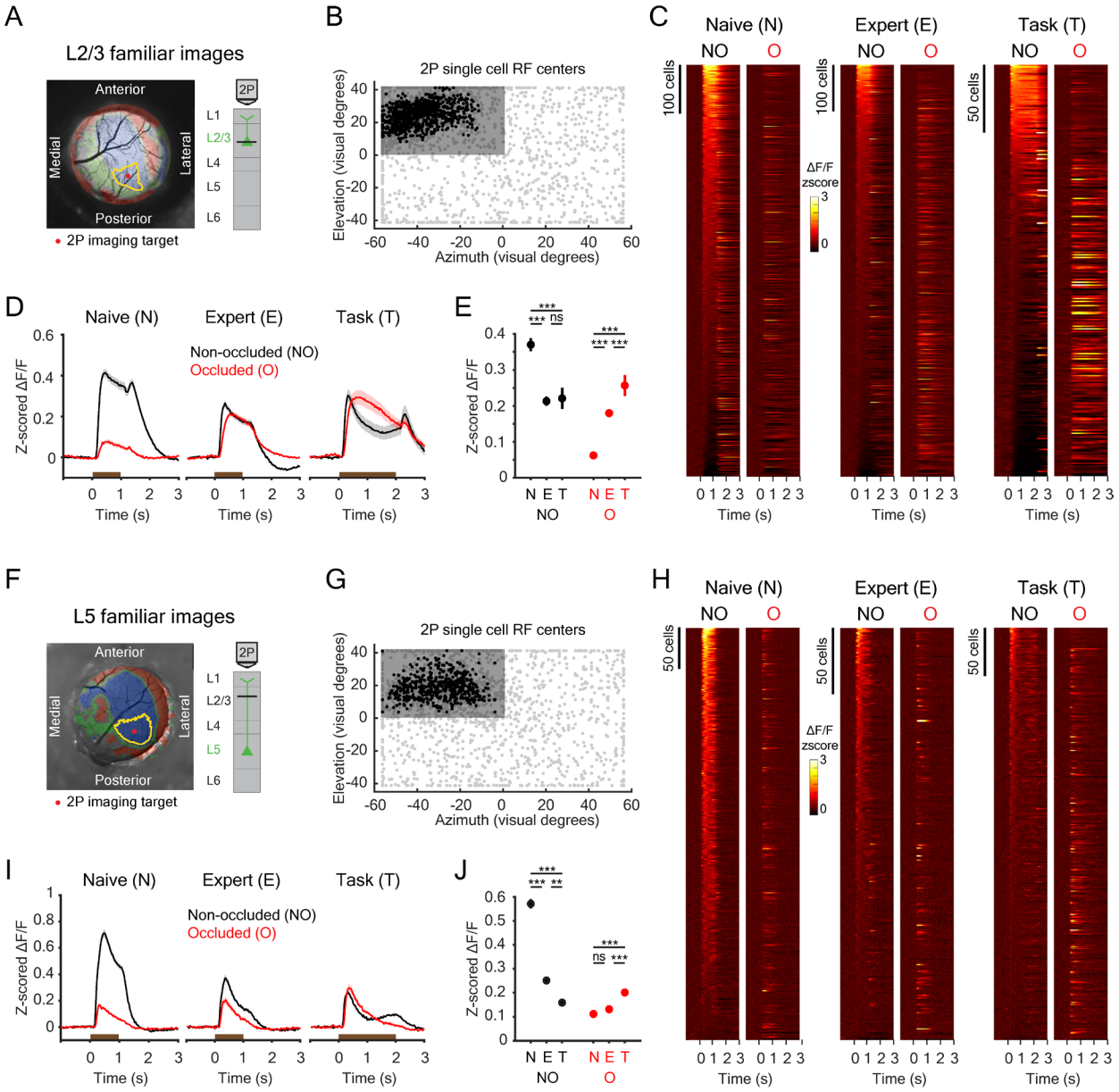

Figure 2. Experience shapes L2/3 and L5 responses to familiar feedforward and contextual inputs.

A) WF field-sign map showing V1 (blue, field-sign = -1) and higher visual areas (red, field-sign = 1) as obtained by population receptive field mapping for an example L2/3 mouse. Green areas represent regions for which the sign could not be determined. The yellow outline indicates the area in V1 that represents the occluded quadrant on the screen. 2P imaging was targeted in the center of this region (red dot).

B) Visual field representation of the stimulus screen showing L2/3 single cell RF centers. Gray dots are excluded RFs and black dots included RFs.

C) Heatmap of z-scored ΔF/F responses for individual L2/3 neurons across conditions and stimuli. Neurons are sorted within each condition (Naive/Expert/Task) based on their average response (t = 0.2-1 s) to the non-occluded stimuli. N = 841 neurons (Naive), 884 neurons (Expert) and 300 neurons (Task) from 6 mice. NO: non-occluded, O: occluded.

D) Z-scored ΔF/F traces averaged across L2/3 neurons and stimuli for all conditions. Brown bars indicate stimulus epoch.
E) Mean response strength across stimuli and conditions (mean ± SEM, averaged between t = 0.2-1 s). LMEM with post hoc Tukey HSD for all comparisons, ***: $p<0.001$, ns: not significant.
F) As in A, but for L5 neurons.
G) As in B, but for L5 neurons.
H) As in C, but for L5 neurons. N = 497 neurons (Naive), 308 neurons (Expert) and 422 neurons (Task) from 5 mice.
I) As in D, but for L5 neurons.
J) As in E, but for L5 neurons. LMEM with post hoc Tukey HSD for all comparisons, ***: $p<0.001$, **: $p<0.01$, ns: not significant.

Locomotion is known to modulate visual responses in mouse V1[25,26]. As mice may alter their running behavior over time, this could potentially affect the responses to non-occluded or occluded images and partially explain their changes. We used two approaches to test whether locomotion influenced plasticity of responses to non-occluded and occluded stimuli. First, we removed the contribution of locomotion by using the residual neural activity after regressing out running speed (Figure S2A-S2B). Second, we removed all trials in which the average running speed of the mouse exceeded 2 cm/s (Figure S2C-S2D). Both approaches resulted in a reduction of the overall response strengths of L2/3 and L5 PyCs but did not alter the relative changes induced by visual experience. Thus, the experience-dependent changes in visual responses in L2/3 and L5 PyCs were not caused by altered running behavior of the mice.

We conclude that visual experience decreased responses of L2/3 PyCs to non-occluded images, while it increased responses to occluded images. Although L5 PyCs in expert mice also showed a strong response reduction to the non-occluded familiarized images, we did not measure the same level of plasticity for responses to occluded stimuli. Finally, task engagement enhanced responses to occluded images in both layers, suggesting that it strengthens contextual inputs.

Separation of L2/3 PyCs responding to feedforward and contextual information

We next analyzed how responses to non-occluded and occluded images were distributed across neurons. Interestingly, many L2/3 PyCs appeared to respond to either the non-occluded stimulus or the occluded stimulus but not to both, especially in expert mice and during task engagement

(Figures 2C and 3A-3B). To quantify the extent of this unexpected separation of neurons into two non-overlapping populations, we computed a separation index (SI) ranging from -1 to 1. The SI is positive if the degree of separation is higher than expected if the activity elicited by non-occluded and occluded stimuli is uncorrelated across neurons. The SI is negative if both categories of stimuli activate the same neurons. The SI increased with experience and task engagement (Figure 3A-B, SI: 0.040 for naive, 0.426 for expert and 0.874 for task). In parallel, the correlation coefficient (R) between average responses to non-occluded and occluded stimuli decreased (R: 0.139 for naive, -0.036 for expert, -0.111 for task), affirming the difference in responses to the two types of stimuli.

One explanation for the observed separation into two populations could be that the different non-occluded or occluded images simply stimulated neurons that preferred different visual stimuli in their cRF, just like neurons responded preferentially to different non-occluded images. To test this and to better understand the relation between responses to pairs of individual images (i.e. image 1 and image 2), we next performed correlation analyses on responses to all possible pairs of the four familiar images that were both occluded (O-O), both non-occluded (NO-NO) or of which one was non-occluded and the other occluded (NO-O). For instance, for the O-O condition, we computed the correlations between the responses of all neurons recorded in one mouse to each pair of occluded images (i.e. O_1 versus O_2, O_1 versus O_3, etc., 6 pairs in total). We then averaged these correlations to obtain a mean correlation per mouse. For the NO-O condition, we computed the correlation coefficient for all pairs of images as described above and also included the correlation between the non-occluded and occluded version of the same images (NO_1 versus O_1, NO_2 versus O_2, etc., 16 pairs in total). We repeated this process for all conditions (naive, expert and task), resulting in the graph in Figure 3C. The correlations of L2/3 PyC population responses to non-occluded and occluded images (NO-O) were lower than the correlations of population responses to different non-occluded images (NO-NO, Figures 3C and S3-S4). This suggests that the separation into two populations is not explained by simple differences in the tuning properties of the neural populations for feedforward cRF inputs. We also found that responses to pairs of occluded images (O-O) were most strongly correlated. This suggests that although some L2/3 PyCs respond preferentially to some of the occluded images,

activity elicited by occluded stimuli represents a signal that is much more similar across images than the signal for non-occluded stimuli.

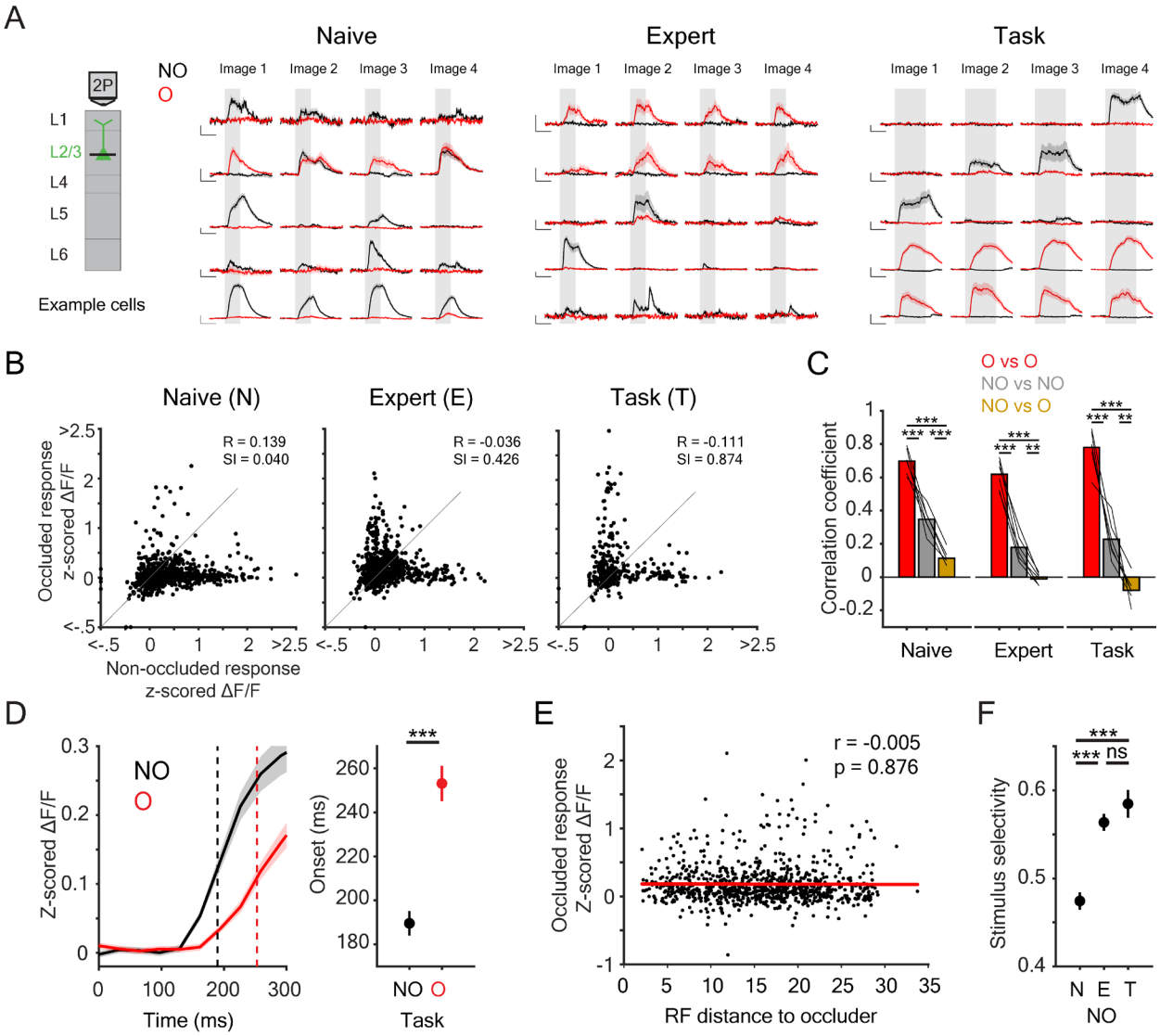

Figure 3. Separation of visual and contextual responses in L2/3

A) Neuronal responses of example L2/3 neurons to the familiar images. The neurons in the three panels from a naive mouse, an expert mouse and a mouse engaged in the task are different. NO, non-occluded; O, occluded. Scale bars, 1 s, 1 z-scored ΔF/F. The shaded bars indicate stimulus epochs.

B) Scatter plot showing average z-scored ΔF/F responses (t = 0.2-1 s) to the non-occluded (x-axis) and occluded (y-axis) stimulus across conditions. N = 841 neurons (Naive), 884 neurons (Expert) and 300 neurons (Task) from 6 mice. R, correlation coefficient; SI, separation index.

C) Mean correlation coefficients of population responses between individual images within (NO-NO and O-O) or between (NO-O) stimulus conditions. Lines represent individual animals (n = 6). ANOVA with post hoc Tukey HSD for all comparisons, ***: p<0.001, **: p<0.01. NO: non-occluded, O: occluded.

D) Left: zoom of mean response to NO and O images across neurons during task performance (mean ± SEM). Dotted lines represent mean onset times. Right: quantification of onset times (NO: n = 142 neurons, O: n = 174 neurons). LMEM for all comparisons, ***: p<0.001.
E) Scatter plot showing the relationship between the distance between RF edge and the border of the occluder and the response to occluded stimuli. The linear regression line is indicated in red.
F) Stimulus selectivity (lifetime sparseness) for responses to non-occluded stimuli. N = 841 neurons (Naive), 884 neurons (Expert) and 300 neurons (Task) from 6 mice. LMEM with post hoc Tukey HSD for all comparisons, ***: p<0.001.

We next determined the onset latency of the calcium responses to non-occluded and occluded images by fitting a curve to the activity time course and taking the time point at which the curve reached 33% of its maximum[27]. We only included neurons with high quality fits (see Materials and Methods). Although calcium activity rises slower than spiking activity, the responses elicited by occluded stimuli were delayed compared to responses elicited by non-occluded images (Figures 3D, LMEM: 189 ± 5.6 ms for non-occluded and 253 ± 8.0 ms for occluded, $P < 0.001$), in line with the interpretation that responses to occluded images were driven by top-down inputs[12]. Finally, we assessed whether the responses to occluded stimuli could be explained by responsiveness to the nearby edge of the occluded region, in which case the responsiveness should depend on its proximity. However, the correlation between response strength and cRF distance to the edge of the occluded region was weak and statistically non-significant (Figure 3E, $r = -0.005$, $P = 0.876$), excluding this explanation (in line with human fMRI and monkey recordings[7,12]).

Taken together, our results show that activity driven by non-occluded and occluded images occurs in separate populations of L2/3 PyCs. These populations are reminiscent of positive and negative prediction error neurons theorized to exist in L2/3 in the framework of predictive coding[19,28,29].

Responses to feedforward and contextual information in L5 PyCs

It is currently not clear whether L5 PyCs compute responses to absence or presence of expected stimuli in a similar fashion to L2/3 PyCs or whether they play a different role, which could be

related to the representation of an internal model[16,20,30]. We therefore investigated how L5 PyCs responsed to non-occluded and occluded images. The separation of L5 PyCs responding to either non-occluded or occluded scenes was less complete than in L2/3, because more cells responded to both types of stimuli (Figures 4A-4C and S5-S6). Like in L2/3, experience increased the separation between L5 PyCs responding to non-occluded and occluded images (SI: -0.389 for naive and 0.297 for expert), even though it did not strengthen responses to occluded images (Figure 2I). Conversely, task engagement did not increase the separation of L5 PyC populations (SI: 0.297 for expert and 0.204 for task), but did strengthen responses to occluded images as was

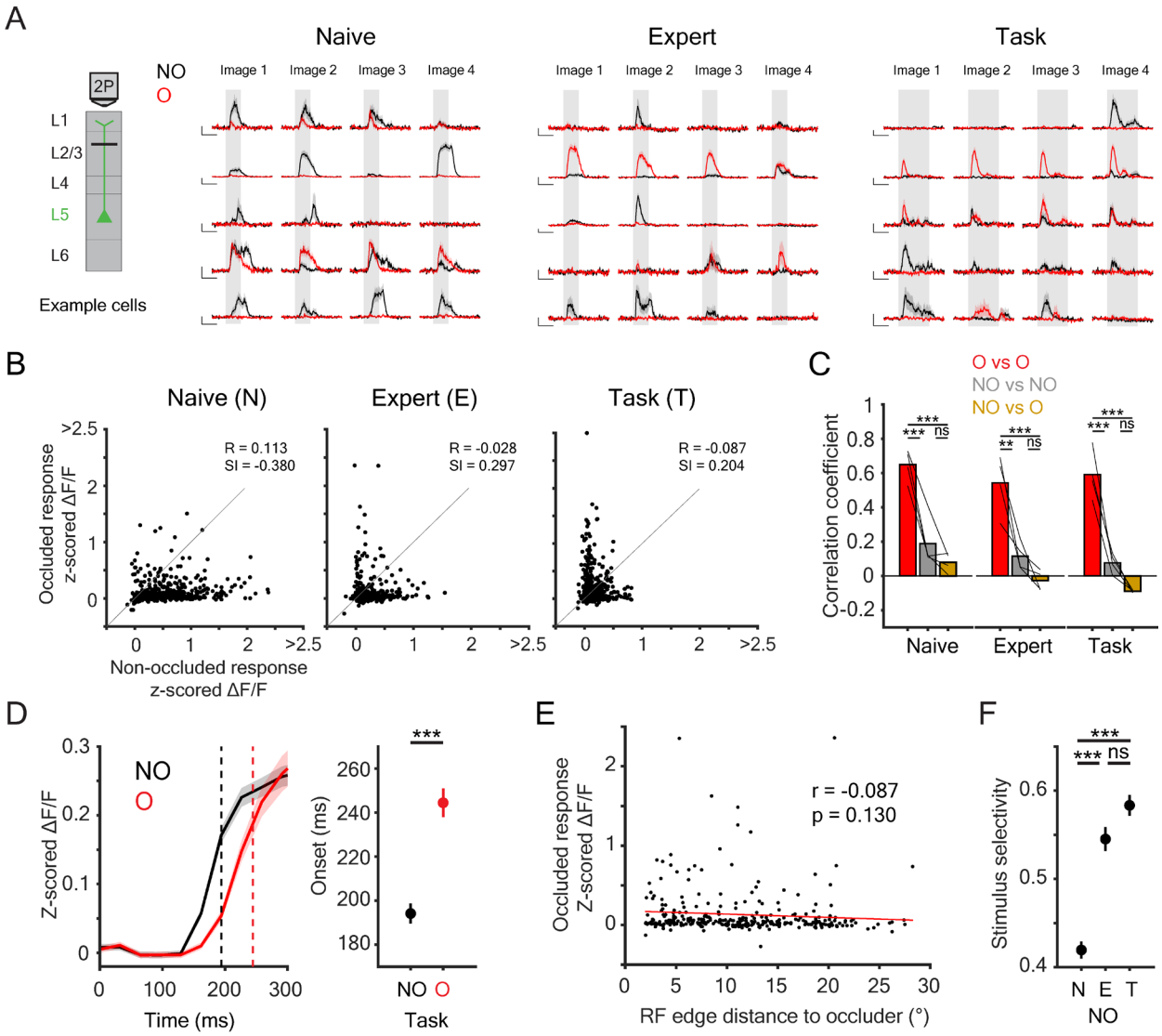

Figure 4. Separation of visual and contextual responses in L5

A) Neuronal responses of example L5 neurons to familiar images. Different neurons are shown in the three panels. NO, non-occluded; O, occluded. Scale bars, 1 s, 1 z-scored ΔF/F.
B) Scatter plot showing average z-scored ΔF/F responses (t = 0.2-1 s) to the non-occluded (x-axis) and occluded (y-axis) stimulus across conditions. N = 497 neurons (Naive), 308 neurons (Expert) and 422 neurons (Task) from 5 mice. R, correlation coefficient; SI, separation index.
C) Mean correlation coefficients of population responses between individual images within (NO-NO and O-O) or between (NO-O) stimulus conditions. Lines represent individual animals (n = 5). ANOVA with post hoc Tukey HSD for all comparisons, ***: p<0.001, **: p<0.01, ns: not significant. NO: non-occluded, O: occluded.
D) Left: zoom of mean response to NO and O images across neurons during task performance (mean ± SEM). Dotted lines represent mean onset times. Right: quantification of onset times (NO: n = 205 neurons, O: n = 159 neurons). LMEM for all comparisons, ***: p<0.001.
E) Scatter plot showing the relationship between RF edge distance to the occluder and the response to occluded stimuli. The linear regression line is indicated in red.
F) Stimulus selectivity (lifetime sparseness) for responses to non-occluded stimuli. N = 497 neurons (Naive), 308 neurons (Expert) and 422 neurons (Task) from 5 mice. LMEM with post hoc Tukey HSD for all comparisons, ***: p<0.001.

discussed in the above (Figure 2I). Finally, like in L2/3, responses to occluded images were delayed in L5 PyCs (Figure 4D, LMEM: 194 ± 4.6 ms for non-occluded and 244 ± 6.5 ms for occluded) and we observed no correlation between the strength of these responses and the cRF distance to the occluder (Figure 4E, r = -0.087, P = 0.130). We conclude that L5 PyC responses to non-occluded and occluded images are less separable, and depend more on engagement in the task.

Selectivity of responses to non-occluded images increases with experience

A reduction of responses to expected and frequently presented stimuli is a known and robust effect[31–36], but it is debated whether this primarily affects the most selective or the least selective neurons, causing dampening or sharpening of the responses, respectively. We therefore tested how the stimulus selectivity (lifetime sparseness, which measures the selectivity of a neuron's response to different stimuli) for non-occluded images changed after familiarization and found that it increased in both L2/3 and L5 (Figure 3F and 4F, LMEM: L2/3 naive versus expert $P < 0.001$ and L5 naive versus expert $P < 0.001$). We next asked whether the change in response strength that neurons displayed due to familiarization depended on their selectivity for non-occluded

images before training. For this, we matched neurons across chronic imaging sessions and correlated stimulus selectivity for non-occluded images in naive mice with their change in activity (ΔF/F naive - ΔF/F expert) (Figure S7). This correlation was negative and significant for both L2/3 and L5 neurons (L2/3: r = -0.299, *P* = 0.001, L5: r = -0.263, *P* = 0.005). Thus, familiarization results in an increase in the selectivity of L2/3 and L5 PyC responses and this can be explained by the stronger suppression of weakly selective neurons that were more likely to respond to each image.

Occluded stimuli elicited stimulus-specific neural signatures across species

In humans and non-human primates, natural scenes elicit stimulus-specific activity from which the identity of the image can be decoded, and remarkably, decoding is even possible if the neurons' cRFs fall on the occluder[7,9,12]. Furthermore, a linear classifier (linear discriminant analysis; LDA) trained on responses to non-occluded scenes can generalize to responses to occluded images and vice versa. This successful cross-decoding suggests that responses to non-occluded and occluded stimuli contain overlapping information and have a similar structure. The observation that responses to non-occluded and occluded images occurred predominantly in separate populations of L2/3 and L5 PyCs in mouse V1 is surprising in this context, inviting the question of whether this separation would prevent cross-decoding in mice.

To address this question, we performed a population classification procedure using all neurons after averaging responses for each neuron and each trial (between 0.2-1 s after stimulus onset). We used 50% of the trials to train the classifier and the 50% remaining trials for testing. Training and testing the classifier on either non-occluded (Train-Test, i.e. NO-NO) or occluded (O-O) responses allowed us to examine whether these signals contain stimulus-specific information. In addition, we examined generalization by performing cross-decoding by training the classifier on one condition and testing it on the other (NO-O or O-NO).

The linear classifier performed above chance level in almost all conditions, especially when we used a time-based classification procedure (Figures 5 and S8). Remarkably, decoding performance across conditions in mice was strikingly similar to that in humans and non-human primates (Figure 5B-C), despite the differences in species and recording techniques. We observed

high (>80%) and significant decoding of responses to non-occluded stimuli (NO-NO) across all species and layers. O-O decoding accuracy was lower but significant, showing that occluded stimuli elicited stimulus-specific V1 responses in mice (Figure 5A,C), just like in humans and non-human primates (Figure 5B-C). Finally, across all species and conditions, we observed that classifiers trained on occluded responses and tested on non-occluded responses (O-NO) were more accurate than the other way around. Possibly, the classifier trained on non-occluded images preferentially makes use of feedforward responses to decode the images, which are absent in the responses to occluded images. The classifier trained on occluded images depends on contextual responses that may also weakly contribute to responses to non-occluded images, allowing slightly better cross-decoding. Together, these results show that L2/3 and L5 PyC responses to the occluded images contain information about the content of the scenes and that above-chance cross-condition decoding is possible despite the separation of populations of PyCs responding preferentially to non-occluded or occluded images.

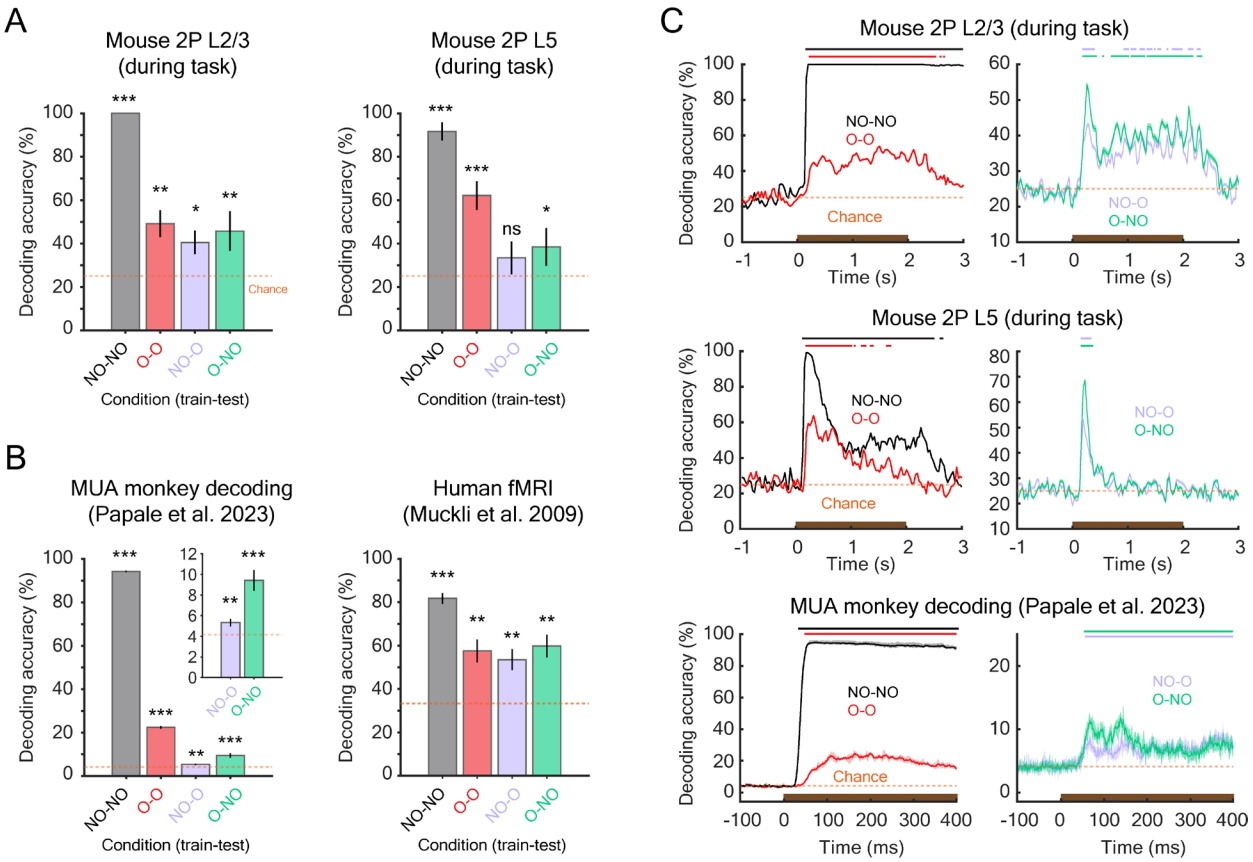

Figure 5. Responses to occluded scenes contain stimulus-specific information in mouse, monkey and human visual cortex.

A) Accuracy of population decoding of stimulus identity for mouse L2/3 PyCs (left, n = 300 PyCs) and L5 PyCs (right, n = 422 PyCs) during the task. An LDA decoder was trained and tested on separate sets of trials for cross-validation (NO-NO, O-O) or cross-decoding (NO-O, O-NO). Bars show mean ± SEM across repetitions of decoding runs. Chance performance (orange dashed line) was 25%. Permutation test, ***: p<0.001, **: p<0.01, *: p<0.05, ns: not significant. NO: non-occluded, O: occluded.
B) Left: decoding accuracy for MUA monkey data. Chance performance was 4.16%. Permutation test, ***: p<0.001, **: p<0.01. Bars show mean ± SEM across repetitions of decoding runs. Inset shows a zoom for NO-O and O-NO conditions. Right: decoding accuracy for human fMRI data. Chance performance was 33.3%. Bars show mean ± SEM across individual subjects (n = 6). T-test against chance, ***: p<0.001, **: p<0.01.
C) Population decoding accuracy over time for mouse L2/3 PyCs (top), L5 PyCs (middle) and monkey MUA (bottom). Colored dashes at the top depict significant time points (p<0.05, permutation test). Brown bars indicate the time window with the visual stimulus. Orange dashed line represents chance performance.

We also found that experience significantly increased the decoding performance of occluded images in both L2/3 and L5 PyCs (permutation test: L2/3 naive versus expert: 18.3% increase, $P < 0.001$; L5 naive versus expert: 24.7% increase, $P < 0.001$). This suggests that stimulus-specific memory traces are encoded in a subpopulation of L2/3 and L5 PyCs that signal the expectation of stimulus-specific information that is missing. We conclude that responses of PyCs to non-occluded and occluded images encode image-specific information and are highly similar across species.

Novelty induces strong activity in mouse V1

The strengthening of responses to occluded images after mice are familiarized with non-occluded images aligns with the notion that they signal the absence of a predicted stimulus, as familiarization presumably strengthens the prediction. The weakening of responses to non-occluded images in the same mice is in accordance with the notion that they signal the appearance of a stimulus that is predicted more strongly after familiarization. If this interpretation is correct, responses to stimuli with which the mice were not familiarized should not weaken when non-occluded, nor strengthen when occluded, as they remain unpredicted. However, there is also evidence suggesting that responses to incorrectly predicted stimuli result in amplified responses, caused by surprise or error signals broadcast from higher order brain

regions[36,37]. In this case, responses to occluded or non-occluded images with which the mice were not familiarized may actually strengthen.

To test these hypotheses, we focused on the subset of images that was omitted from the training regime (novel condition). L2/3 PyC responses to novel, non-occluded images in expert mice were not weakened but strongly increased after familiarization with the other images (Figure 6A-6D, LMEM: naive versus expert, $P < 0.001$). This thus suggests that a surprise or error signal contributes to these responses. To test whether neurons responding to the novel images predominantly signaled surprise that was not related to the content of the images, we assessed whether they also responded to familiar occluded images, which were also not predicted and should then also cause surprise. However, correlations between responses to familiar occluded and novel non-occluded images were weak and much lower than between different occluded stimuli (Figure 6D), suggesting that the responses did not signal non-selective surprise but represented an amplified selective response.

Responses to novel images that were occluded were also stronger in expert mice than in naive mice (Figure 6A-C, LMEM: naive versus expert, $P < 0.001$). This suggests that the occlusion caused an amplified response that did not depend on the exact content of the missing information. This predominantly involved the same neurons that also responded to familiar occluded images (Figure 6E), mirroring the observation that responses to different occluded images are correlated (Figure S4). We observed a similar increase in responses to novel non-occluded stimuli in L5 (Figure 6F-J). However, responses to novel occluded images did not significantly increase after training (LMEM: naive versus expert, $P = 0.450$), similarly to the responses to familiar occluded images (Figure 2J).

Taken together, these results show that responses to images to which the mice were not familiarized increase after the training sessions, as do responses to these images when partially occluded. Both observations do not align with the idea that the responses represent locally computed prediction errors that signal the difference between the feedforward input and the top-down prediction, as neither of them should have changed. The data better match the idea

that incorrectly predicted stimuli result in amplified responses, caused by surprise or error signals broadcast from higher order brain regions[36,37].

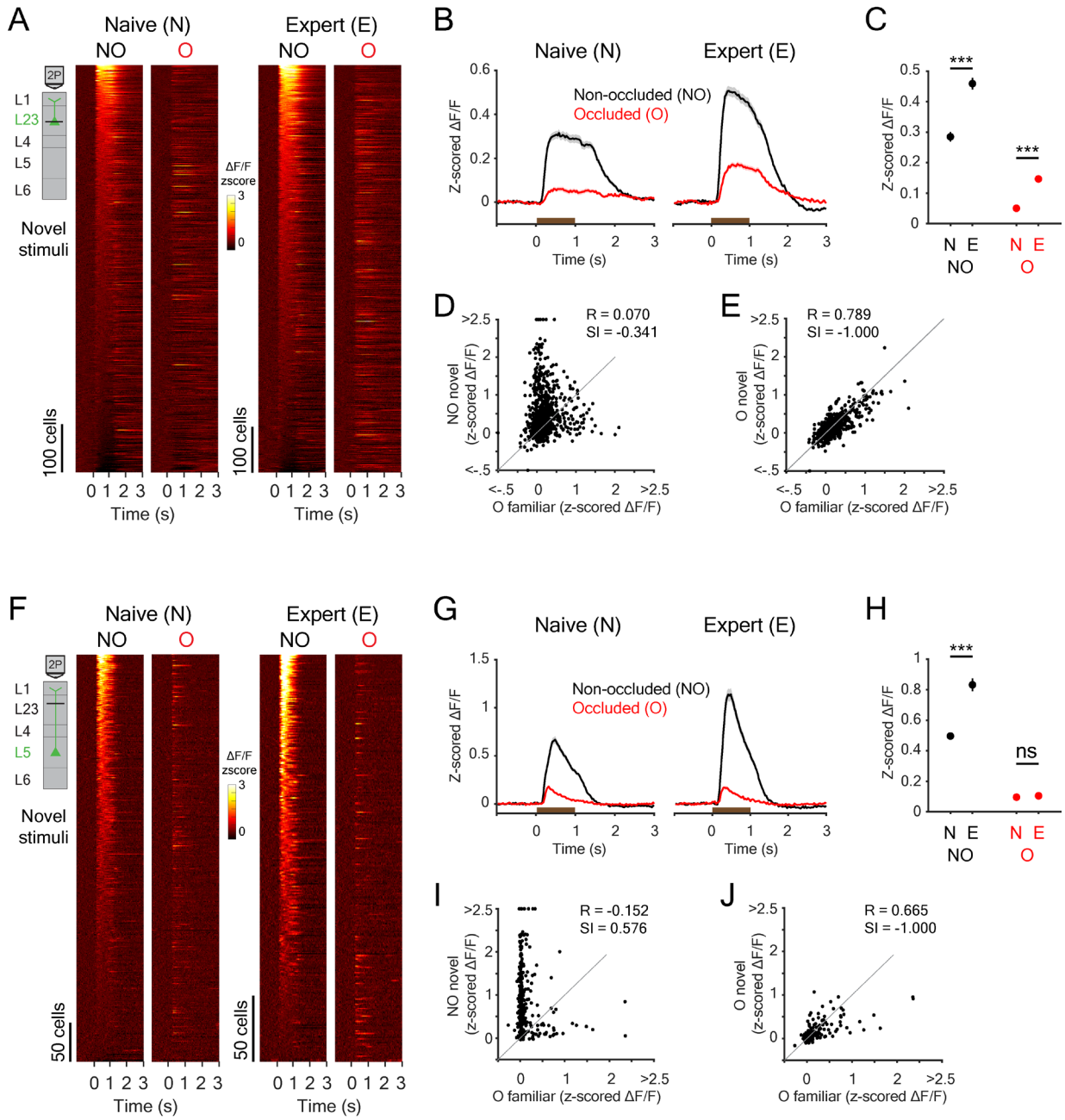

Figure 6. Experience shapes L2/3 and L5 responses to novel feedforward and contextual inputs

A) Heatmap of z-scored ΔF/F responses for individual L2/3 neurons across conditions and stimuli for novel images. Neurons are sorted within each condition (N/E/T) based on their average response (t = 0.2-1 s) to

the non-occluded stimuli. N = 841 neurons (Naive), 884 neurons (Expert) and 300 neurons (Task) from 6 mice.

B) Z-scored ΔF/F traces averaged across neurons and stimuli for novel images. Brown bars indicate the visual stimulus.
C) Mean response strength across stimuli and conditions (mean ± SEM, averaged between t = 0.2-1 s). LMEM for all comparisons, ***: p<0.001.
D) Scatter plot showing average z-scored ΔF/F responses (t = 0.2-1 s) to occluded familiar stimuli (x-axis) and non-occluded novel stimuli (y-axis).
E) Scatter plot showing average z-scored ΔF/F responses (t = 0.2-1 s) to occluded familiar stimuli (x-axis) and occluded novel stimuli (y-axis).
F) As in A, but for L5 neurons. N = 497 neurons (Naive), 308 neurons (Expert) and 422 neurons (Task) from 5 mice.
G) As in B, but for L5 neurons.
H) As in C, but for L5 neurons. LMEM for all comparisons, ***: p<0.001, ns: not significant.
I) As in D, but for L5 neurons.
J) As in E, but for L5 neurons.

DISCUSSION

Making use of a paradigm in which we recorded V1 responses to non-occluded and partially occluded natural images, we demonstrate that PyCs respond to contextual visual information in the absence of feedforward inputs and that visual experience drives memory traces related to the presented scenes. Experience with the image material results in enhanced signals when unfamiliarized images are added to the stimulation set or when image information that is predicted is withheld because it is occluded. Furthermore, we show that responses to occluded and non-occluded images occur in separate populations of L2/3 PyCs and that experience and task engagement strengthen this separation. In L5, PyCs also respond to non-occluded and occluded scenes, but the separation of populations responding to these types of stimuli is less pronounced than in L2/3 PyCs. Moreover, visual experience does not significantly enhance responses to the occluded scenes in L5.

Based on previous work, this separation of responses to non-occluded and occluded scenes is surprising. Studies using this occlusion paradigm in human subjects[9] and non-human primates[12] have shown that classifiers trained on V1 responses to occluded images can successfully decode responses to the non-occluded images. This suggests that neurons responding to a non-occluded image might also receive top-down contextual inputs about that image when it is partially

occluded. Indeed, this type of organization underlies figure-ground modulation, where the response to a feedforward stimulus is enhanced when it is part of a figure[1,2,38]. The enhancement occurs predominantly after the initial peak of the response and depends on top-down inputs from higher-order visual areas[1,2,38]. Similarly, PyCs not only respond when visual stimuli are presented within their cRF, but also when a stimulus surrounds it[26,39]. These inverse receptive field responses are slightly delayed, and driven by extraclassical RF inputs provided by feedback from higher-order areas[39]. Together, these observations suggest that under these experimental conditions, feedforward and contextual top-down inputs are processed by the same PyCs.

The separation of PyC populations that respond to non-occluded or occluded natural scenes is more reminiscent of recent findings related to visuomotor processing in L2/3 of V1[19,29]. In these studies, mice were placed in a virtual tunnel in which the visual flow was sometimes stopped while the mice were still running, or visual flow started while mice were stationary. Separate neural populations were identified that either responded to visual flow or to unexpected halting of the flow during running. It was suggested that these neural populations represented positive and negative prediction error neurons, responding to the unpredicted appearance of visual stimuli or the cessation of predicted locomotion-induced visual flow, respectively. In a parallel fashion, the responses to occluded images may signal the absence of expected information, while the responses to non-occluded images could signal the appearance of an unpredicted visual stimulus.

A relevant question is whether the PyCs responding to non-occluded or occluded natural images correspond to genetically defined populations of PyCs in V1, such as recently shown for visuomotor prediction error neurons[19]. It is possible that negative prediction error neurons are a genetically defined subpopulation of L2/3 PyCs and include the PyCs responding to occluded images. However, we find that neurons responding to occluded images do respond to cRF stimulation (sparse noise used for RF mapping) and locomotion does not selectively affect responses to occluded or non-occluded images. Therefore, we believe that the PyCs that respond to occluded stimuli may not belong to the same genetically defined subset as visuomotor mismatch cells. Similarly, intracortical and pyramidal tract projecting PyCs in L5 also show distinct responses to visuomotor mismatch and visual stimuli[40]. To understand how predictive signals are

generated and what the underlying neural circuit mechanisms are, it will be crucial to map the visual response properties of neurons in the different cortical layers to their genetic identities and how these overlap for different types of prediction errors.

The responses to occluded images contain information about the missing content, because a classifier trained on the responses to occluded images could be used to decode the same images when they were non-occluded. The information about the occluded region is probably driven in part by extraclassical RF input[27] and related to spatial expectations, such as the continuation of lines or textures[7]. The strengthening of the responses to occluded images and the increased decoding efficiency after familiarization suggests a strengthening of the contextual information based on visual memory. However, our observation that after familiarization, responses to occluded novel images also increase implies that a surprise or error signal broadcast by higher cortical or thalamic regions also contributes to the amplification of the responses to occluded images[15,36,37].

We found that responses to non-occluded novel images were stronger than those to familiar images. This phenomenon has been observed before and is in line with the expectation that positive prediction errors are stronger for unpredicted stimuli than those to (partially) predicted ones[41–43]. It is surprising though, that the responses to the novel images are stronger than before familiarization, as in both situations the presentation of the image is not predicted. Intuitively, it makes sense that an event that differs from what you expect (i.e. an unfamiliar building in a familiar street) is more surprising than an event that is not expected at all (an unfamiliar building in an unfamiliar street). However, it does not match a model of subtractive prediction error coding in which the prediction error is locally computed by subtracting the prediction from the actual sensory input[14,16,44]. It seems more likely that the strengthening of the response to the novel images is the result of a surprise or error signal that is not computed locally, but at a higher cortical level and broadcast down, amplifying the original response to the same image before training[15,37]. Mechanistically, this could involve disinhibition mediated by VIP interneurons receiving top-down inputs[36,45,46].

Familiarization caused responses to non-occluded images to decrease. This observation aligns with positive prediction error responses that decrease due to increased top-down predictive signals that activate inhibitory neurons in V1[16]. However, the decreased responses may also be caused by other mechanisms, such as increased feedforward inhibition, reduced excitability or synaptic depression. It has been argued that if responses to visual stimuli reflect positive prediction errors, familiarization would cause activity representing expected input to decrease, resulting in a dampening of responses[33,47–50]. Alternatively, it can be reasoned that at the single neuron level, those cells that are least selective are most likely to fire in response to any visual stimulus, and may thus be suppressed preferentially, resulting in sharpening of V1 responses[32,51]. Our results show that responses are sharpened with experience and that this is caused by preferential suppression of PyCs that are least selective before familiarization. This may be the consequence of expectation suppression, as it is more predictable that these cells will fire and the prediction error thus becomes smaller, but may also be a result of repetition suppression, as these neurons firing more frequently.

Taken together, the L2/3 PyCs responding to non-occluded and occluded images have many properties matching positive and negative prediction error neurons, respectively. However, the increased responses to occluded and non-occluded images with which the mice were not familiarized do not align well with a model of subtractive prediction error coding in which prediction errors are computed locally, as before and after training these images were not predictable and therefore, the difference between the actual visual stimulus and the predicted stimulus should not alter.

It has been suggested that while L2/3 PyCs signal prediction errors, L5 PyCs may represent the internal model and thus how the visual stimuli are perceived[16,30]. According to predictive coding theories, the activity of internal representation neurons would be updated based on the inputs of positive and negative prediction error neurons in L2/3[16,20,30]. L5 PyCs showed a less pronounced separation into populations responding exclusively to occluded or non-occluded images and more often responded to multiple occluded and/or non-occluded images. However, understanding whether their responses better reflect the perception of the mice will require different behavioral paradigms, for example using imaginary contours that have been shown to

be perceived as such by mice[52]. When presenting stimuli containing actual or imaginary contours, internal representation neurons should respond similarly to both, while prediction error neurons should respond differently. Notably, we found that responses to occluded images did not increase after familiarization in L5 when mice were passively viewing, but only when they were actively engaged in the task. It is interesting to speculate that task engagement may enhance the expectation that particular scenes will be presented, strengthening the perception or imagination of these images. Mechanistically, this could involve neuromodulatory signals related to attention such as noradrenergic or cholinergic inputs[53–57], or attention-related disinhibition mediated by VIP interneurons[58,59] (but see[60]).

Strikingly, we find that decoding of non-occluded and occluded images occurs with very similar efficiency across humans, monkeys and mice, despite using fMRI, electrophysiology and 2P calcium imaging, respectively, which are very different neural recording techniques. This suggests that the same neural mechanisms underlie these responses across species. How detailed the predictive information about the occluded natural scenes is remains to be investigated. However, the activity elicited by occluded image regions in V1 of humans, is well described by activity models generated from their line drawings when they are asked to sketch the image region that is occluded[7], suggesting that occlusion signals can be conceptualized as mental line drawings. One way to compare such signals between humans and non-human primates is by means of their representational dissimilarity correlation. Time resolved representational dissimilarities derived from non-human primate V1 recordings with fMRI signals of human occluded V1 start to correlate after 100 ms[12]. This suggests that after that point in time non-human primates may have similar mental representations of the occluded image region as humans.

The occlusion paradigm may thus prove to be a powerful tool for studying predictive coding in the visual system from the cognitive level in humans to the circuits and molecular level in mice. The results obtained using the occlusion paradigm may be easier to translate to the situation in primates than those using visuomotor mismatch, as recent findings suggest that primates do not display strong locomotion modulation in V1[62]. While predictive coding is becoming a leading theory of how the brain operates, there is a need to better understand the underlying neural circuit mechanisms. The occlusion paradigm will make it possible to study how negative and

positive prediction errors in V1 relate to perception and to situations during which internal models are perceived as real, such as dreaming or hallucinations. These insights will be crucial for understanding the mechanisms of perception and the pathophysiology of brain disorders such as schizophrenia in which perception is distorted.

MATERIALS AND METHODS

Mice

All experiments were approved by the institutional animal care and use committee of the Royal Netherlands Academy of Arts and Sciences. For L2/3 experiments we used 4 female and 2 male G35-3Dtl[21] crossed to AI93 TITL-GCaMP6f mice (Jackson Laboratories, www.jaxmice.jax.org, strain 024107). For L5 experiments we used 2 female and 4 male Rbp4-Cre mice (line KL100, GENSAT project), of which one male mouse was only used for wide-field imaging. This mouse line B6.FVB(Cg)-Tg(Rbp4-cre)KL100Gsat/Mmucd, RRID:MMRRC_037128-UCD, was obtained from the Mutant Mouse Resource and Research Center (MMRRC) at University of California at Davis, an NIH-funded strain repository, and was donated to the MMRRC by MMRRC at University of California, Davis. Made from the original strain (MMRRC:032115) donated by Nathaniel Heintz, Ph.D., The Rockefeller University, GENSAT and Charles Gerfen, Ph.D., National Institutes of Health, National Institute of Mental Health. Mice were group housed under a 12 h reversed day/night cycle and provided with ad libitum access to food and water. Experiments were performed in the dark phase. Mice had access to a running wheel in their home cage throughout the experiment.

Window surgery and viral injections

For the cranial window surgery, mice were anesthetized with isoflurane (4% induction, 1.6% maintenance in oxygen). During the surgeries, temperature was maintained at 37°C with euthermic pads and eyes were protected from light and drying using Cavasan eye ointment. Mice were implanted with a double (3+4 mm diameter) glass window and a custom metal head-ring

on the center of V1 to allow head-fixation. The glass window and head-ring were fixed to the skull using dental cement. One week after window surgery, mice used for L5 experiments were injected with 100 µl AAV-PHP-eB-CAG-dlox-GCaMP6f-dlox (VVF Zurich, final titer ~10E12) in their tail vein while they were awake and body restrained. At least one week after the window surgery or viral injection, mice were handled and trained to be head immobilized in our setup until they sat comfortably and started running regularly on their own.

Two-photon imaging

Two-photon experiments were performed on a two-photon microscope (Neurolabware) equipped with a Ti-sapphire laser (Mai-Tai 'Deepsee', Spectraphysics; wavelength, 920 nm) and a 16x, 0.8 NA water immersion objective (Nikon) at a zoom of 1.6x (for L2/3 somas) or 2x (for L5 dendrites). The microscope was controlled by Scanbox (Neurolabware) running on MATLAB (Mathworks). Images were acquired at a frame rate of 15.5 (RF mapping) or 31 Hz (occlusion experiments). For all behavioral training and imaging sessions, mice were head restrained and free to run on a 3D-printed running wheel (8.5 cm diameter). Locomotion speed was measured with a rotary encoder and processed using Arduino and MATLAB.

All visual stimuli for two-photon imaging were presented on a 24-inch gamma-corrected non-occluded HD LED monitor (1920x1080 pixels) using OpenGL and Psychophysics Toolbox 3 running on MATLAB. The monitor was positioned centered at 15 cm away from the mouse, yielding a field-of-view of 120° x 90°.

For RF mapping, we used eccentricity-corrected sparse noise stimuli with squares of 7.5 visual degrees at different locations covering the entire screen. Each trial consisted of 3 black and 3 white randomly positioned squares on a gray background. Stimuli were presented for 0.5 s with a gray screen ITI of 1.5 s.

For occlusion experiments, we presented 6 natural images that were part of a dataset used for similar experiments before[7,12]. The images were presented in gray scale and were corrected for overall luminance across images. We presented images non-occluded or partially occluded using

a gray occluder positioned on the top left quadrant of the screen. The occluder had identical luminance to the ITI gray screen. Non-occluded and occluded images (50% of trials each) were both presented 20 times for 1 s with a random ITI of 4-6 s.

Wide-field imaging

Wide-field imaging was performed as described as before[63]. Briefly, we imaged the entire 3 mm window using a wide-field fluorescence macroscope (Axio Zoom.V16 Zeiss/Caenotec-Prof. Ralf Schnabel). The mouse was positioned in the center of the LCD screen. Images were captured at 20 Hz by a high-speed sCMOS camera (pco.edge 5.5) and recorded using the Encephalos software package (Caenotec-Prof. Ralf Schnabel).

All visual stimuli used for wide-field imaging were created and presented using COGENT (developed by John Romaya at the LON at the Wellcome Department of Imaging Neuroscience) running in MATLAB as described before[63]. In short, mice were positioned 14 cm away from a 122 × 68 cm LCD screen (Iiyama LE5564S-B1), resulting in a field-of-view of 144° x 86°. The screen had a resolution of 1920 × 1280 pixels running at refresh rate of 60 Hz. Stimuli used for pRF mapping were as described before[63] and consisted of eccentricity-corrected angled bars (at 0°, 45°, 90° or 135°, 10° in diameter) of a checkerboard pattern on a gray (20 cd/m^2) background. The total number of 58 stimuli were presented 10 times each for 0.5 s followed by a gray (20 cd/m^2) ITI of 3.6 s. Natural stimuli used for wide-field occlusion experiments were similar as for two-photon experiments (described above). Both non-occluded and occluded images were presented 20 times for 1 s with an ITI of 4-6 s.

Behavioral training and analysis

For behavioral training, water-deprived mice were trained to detect 4 out of 6 non-occluded images to make them familiar. The remaining 2 novel/untrained images were not shown during training. Mice were free to run on the wheel while images were presented for 2 s with a random inter-trial interval of 7-10 s. In the initial passive stage of the training, mice were rewarded with

a 5 µl water drop 1 s after stimulus offset. When mice started to lick before the reward delivery, training became active, and a water reward was delivered only when the mice licked in the time window 1-2 s after stimulus offset. Imaging was performed when mice consistently managed to obtain a reward on >70% of trials (generally between 20-30 sessions of 100-200 trials each). Mice continued to be trained in between imaging sessions until the experiments were completed.

The hit rate was defined as:

$$Hit\ rate = \frac{N_{hits}}{N_{hits} + N_{misses}}\ x\ 100\% \qquad 1.$$

The lick index was defined as:

$$Lick\ index = \frac{Lick\ rate_{stim} - Lick\ rate_{ITI}}{Lick\ rate_{stim} + Lick\ rate_{ITI}} \qquad 2.$$

Where $Lick\ rate_{stim}$ is the average lick rate (licks/s) in the 3 s after stimulus onset and $Lick\ rate_{ITI}$ is the average lick rate in the 3 s before stimulus onset.

Wide-field imaging analysis

Captured images (1600x1600 pixels, 20 Hz, 50 ms exposure) were down sampled to 800x800 pixels. Images were then smoothed using a Gaussian filter with a standard deviation of 2 pixels and stored in a trial based format (400 x 400 x time x number of trials). Analysis of pRF mapping and field-sign was performed as described in detail before[63].

For analysis of occlusion experiments, images were semi-automatically registered using intensity-based rotation and translation to the pRF mapping session[63]. Using the pRF map, we extracted signals for the retinotopic region of V1 corresponding to the occluded quadrant of the screen (with a margin of 7 visual degrees to limit contamination from nearby non-occluded regions of V1). We averaged ΔF/F signals for all pixels in the occluded region and calculated the baseline-corrected (average activity in the 0.2 s before stimulus onset) mean traces across trials and conditions.

Two-photon imaging analysis

We used the SpecSeg toolbox for preprocessing as described in detail before[64]. In short, we performed rigid motion correction using NoRMCorre[65] followed by automated region-of-interest (ROI) selection based on cross-spectral power across pixels. After manual refinement, raw ROI signals were extracted and corrected for neuropil by subtracting the average pixel values in an area surrounding each ROI multiplied by 0.7. ΔF/F traces were made by subtracting a moving baseline (10th percentile over 5000 frame windows) and dividing by a linear fit over that baseline.

For RF analysis, we performed reverse correlation on the responses to the sparse noise stimuli to create a 2D response matrix for both the ON (white squares) and OFF (black squares) stimuli. We then fit a circular 2D Gaussian to the response matrix to estimate the RF center and size (full width at half maximum). The quality of the fit was estimated using r^2 and the Signal-to-Noise Ration (SNR).

The SNR was defined as:

$$SNR = \frac{Gauss_{peak} - Gauss_{baseline}}{\sigma_{background}} \quad 3.$$

Where $Gauss_{peak}$ is the maximum of the Gaussian fit, $Gauss_{baseline}$ is the offset parameter and $\sigma_{background}$ is the standard deviation of the background data points (>2 standard deviations away from the center of the Gaussian).

We included neurons if either their ON or their OFF RF met the following criteria: (i) their RF was reliable ($r^2 > 0.33$ for L2/3, $r^2 > 0.15$ for L5 and SNR > 4) and (ii) the edge (based on the FWHM) of their RF was at least 2 visual degrees away from the bottom and right-side edges of the occluder. We used a lower r^2 threshold for L5 neurons to match their lower overall average r^2 scores compared to L2/3 neurons. We did not find any major differences in the results when using $r^2 > 0.33$. For display purposes (Figure 2), we used the ON RF for each neuron whose RF met criteria for both the ON and OFF RF map. For neurons recorded in naive and expert mice, we used RFs

obtained from sparse noise stimuli shown directly before the occlusion stimuli. For the L2/3 task data, we used RFs obtained from the expert RF mapping session by matching neurons between the expert and task dataset. For L5 PyCs, we mapped RFs directly after the task session.

For 2P response strength analyses, we first z-scored ΔF/F signals for each neuron. To compare mean response traces for individual neurons (Figure 2C), we then averaged across repetitions per image followed by stimulus type (NO and O). To compute single cell average response strengths, we took the baseline-corrected (average 1 s before stimulus onset) mean response between t = 0.2-1 s after stimulus onset.

To estimate the relationship between population responses to non-occluded and occluded stimuli across different conditions (Naive, Expert, Task), we calculated the correlation coefficient (R) and the separation index (SI). We calculated the SI as follows. First, we divided the 2D scatter plot (Figure 3B) into four quadrants (2 x 2). We independently defined the borders between the quadrants for the x-axis and y-axis as the mean + 0.75*STD for the non-occluded and occluded responses, respectively. Second, we counted the number of neurons whose response profile was located in the top right quadrant. To estimate the degree to which non-occluded and occluded responses were separated, we compared the neuron count in the upper right quadrant of the real distribution to the same count in a non-correlated distribution with independent sampling for the x and y-coordinate. For this, we ran 10,000 repetitions of the count while each time randomly shuffling the non-occluded and occluded responses (creating random pairs of x and y values), resulting in a distribution of permutation counts. We calculated the separation index (SI) as follows:

$$SI = 1 - \frac{Count_{real}}{MeanCount_{perm}} \qquad 4.$$

Where $Count_{real}$ is the upper right quadrant count from the real data and $MeanCount_{perm}$ is the distribution average of upper right quadrant counts from the permutation data. Values <-1 were clipped at -1. An SI value of -1 represents a separation lower than the chance distribution

(i.e. anti-separation or correlation), 0 represents a lack of separation and 1 represents a separation higher than the chance distribution.

For correlation analyses in Figure 3C and 4C, for each mouse we calculated the population correlation coefficient between responses to different pairs of images. For this, we took all neurons from each mouse (e.g. 100) to the 4 different familiar images as a vector (100 for image 1, 100 for image 2, etc.). For O versus O and NO versus NO, we correlated those 100 responses between pairs of occluded or non-occluded images, respectively (O_1 versus O_2, O_1 versus O_3 etc., 6 pairs in total). For NO versus O, we compared responses between each non-occluded image to each occluded image, also including comparisons between the non-occluded and occluded condition for the same image (NO_1 versus O_1, NO_1 versus O_2 etc., 16 pairs in total). We then averaged all correlations within each mouse to compute the mean value for each mouse.

To correlate the strength of the response to the occluded images with the distance of RF edges to the occluder edge for each neuron, we took either the ON or the OFF RF of the neuron depending on which matched the criteria described above. If both the ON and OFF RFs matched the criteria, we took the ON RF. The distance of the RF edge to the occluder was determined as the shortest of the two possible occluder edges (horizontal or vertical).

We calculated response onset latency for each neuron as described before[27,66] by fitting the sum of an exponentially modulated Gaussian and cumulative Gaussian to the activity time courses for non-occluded and occluded conditions during the task. We defined the onset latency as the time point at which the fitted curve reached 33% of its maximum. We only included neurons with a high-quality fit ($r^2 > 0.5$) and an average response (t = 0.2-1 s) greater than 0.

To estimate the contribution of locomotion to responses and plasticity we used two independent procedures. First, we performed linear regression for each neuron by using locomotion speed as a covariate and neuronal activity as a response variable. We then used the residuals of the model for all subsequent analyses. Second, we repeated the analyses after removing all trials in which the mouse had an average running speed > 2 cm/s during the stimulus window (t = 0.2-1 s).

We defined stimulus selectivity across the 4 different natural images by calculating lifetime sparseness for each neuron as follows:

$$Stimulus\ selectivity = 1 - \frac{(\sum R_i)^2}{N \cdot \sum {R_i}^2} \quad 5.$$

Where R_i represents the neuron's response to the i-th stimulus, and N is the total number of stimuli.

To correlate the change in response strength between naïve and expert conditions to the selectivity to the non-occluded stimulus for individual neurons, we matched neurons across the two recording sessions using the chronic matching module of SpecSeg[64]. We then computed the correlation coefficient using the population of neurons that were found back in both sessions.

Decoding analysis

For population decoding of mouse WF and 2P data and monkey MUA data, we performed LDA using the 'fitcdiscr' function (default parameters) in MATLAB on the neuronal responses to the natural images. We used individual neurons or pixels as predictors for 2P data and WF data respectively. For trial decoding, responses were calculated by taking the baseline-corrected mean ΔF/F from 0.2 to 1 s after stimulus onset for each trial. Decoding of human fMRI data was adapted from Smith & Muckli (2010)[9]. Decoding over time for monkey MUA data was adapted from Papale *et al.* (2023)[12]. For decoding over time using mouse 2P data, we took the baseline-corrected ΔF/F for each frame and each neuron. On each decoding run, we trained an LDA decoder by randomly selecting 50% of the trials and then testing the decoder on the remaining 50% of trials. We repeated this procedure 200 times to account for variability between trials. We built two classifiers, one on non-occluded trials (NO model) and one on occluded trials (O model). We then tested each classifier on both conditions to yield four accuracy scores.

Statistical significance for decoding in individual mice (WF decoding), individual frames (i.e. over time), or the overall population was calculated using a permutation test as described before[12]. We first built a null distribution by repeating the decoding procedure 1000 times with shuffled labels. We then selected the upper tail (highest 30%) of the null distribution, and we fitted a Pareto function to the tail to estimate extreme values[67]. The p-value was identified as the percentile corresponding to the 'real' accuracy value in the null-distribution. To compare the decoding accuracy for O-O between conditions (Naive vs Expert), we used the residuals after regressing out locomotion speed to compute the 200 decoding runs for both conditions and calculated the p-value as described above.

Histology and confocal microscopy

To examine GCaMP expression, mice were perfused with 15 ml of ice-cold PBS followed by 30 ml of 4% paraformaldehyde (PFA). The brains were extracted and post-fixed for 2 h in 4% PFA at 4°C. Brains were cut in 50 µm slices and imaged on an Axioscan.Z1 slide scanner (ZEISS, Germany) at 20X (0.63 NA).

Statistical analyses

All statistical details for each experiment are shown in figures and figure legends and in Supplementary file 1. Unless specified otherwise, statistical analyses were performed using LMEM ('fitlme' function in MATLAB). For LMEM, we considered the response parameter (e.g. visual response magnitude) as the dependent variable, mouse as random effect and the condition (e.g. Naive vs Expert) as the fixed effect. LMEM accounts for the hierarchical correlation structure in the data (i.e. neurons and mice). When the model resulted in a Hessian error (i.e. random effect could not be estimated), we iteratively removed outlier neurons (i.e. neurons with residuals <-2.5 or >2.5 z-score) before refitting the model. For the interaction between cell type (L2/3 vs L5) and condition (Naive vs Expert) in Figure 2, we considered 'cell type*condition' as

the fixed effect. We performed a one-way ANOVA on the LMEM followed by a post hoc coefTest using Tukey's HSD to correct for multiple comparisons.

Literature

1. Lamme, V. A. F. & Roelfsema, P. R. The distinct modes of vision offered by feedforward and recurrent processing. *Trends in Neurosciences* **23**, 571–579 (2000).
2. Roelfsema, P. R. CORTICAL ALGORITHMS FOR PERCEPTUAL GROUPING. (2006).
3. Sillito, A. M., Cudeiro, J. & Jones, H. E. Always returning: feedback and sensory processing in visual cortex and thalamus. *Trends in Neurosciences* **29**, 307–316 (2006).
4. Cauller, L. Layer I of primary sensory neocortex: where top-down converges upon bottom-up. *Behavioural Brain Research* **71**, 163–170 (1995).
5. Muckli, L. & Petro, L. S. Network interactions: non-geniculate input to V1. *Current Opinion in Neurobiology* **23**, 195–201 (2013).
6. Muckli, L. *et al.* Contextual Feedback to Superficial Layers of V1. *Current Biology* **25**, 2690–2695 (2015).
7. Morgan, A. T., Petro, L. S. & Muckli, L. Scene Representations Conveyed by Cortical Feedback to Early Visual Cortex Can Be Described by Line Drawings. *J. Neurosci.* **39**, 9410–9423 (2019).
8. Revina, Y., Petro, L. S. & Muckli, L. Cortical feedback signals generalise across different spatial frequencies of feedforward inputs. *NeuroImage* **180**, 280–290 (2018).
9. Smith, F. W. & Muckli, L. Nonstimulated early visual areas carry information about surrounding context. *Proc. Natl. Acad. Sci. U.S.A.* **107**, 20099–20103 (2010).

10. Petro, L. S., Smith, F. W., Abbatecola, C. & Muckli, L. The Spatial Precision of Contextual Feedback Signals in Human V1. *Biology* **12**, 1022 (2023).

11. Lazarova, Y., Huang, Y., Muckli, L. & Petro, L. S. Perceptual priors add sensory detail to contextual feedback processing in V1. Preprint at https://doi.org/10.1101/2023.09.23.559098 (2023).

12. Papale, P. *et al.* The representation of occluded image regions in area V1 of monkeys and humans. *Current Biology* **33**, 3865-3871.e3 (2023).

13. Clark, A. Whatever next? Predictive brains, situated agents, and the future of cognitive science. *Behav Brain Sci* **36**, 181–204 (2013).

14. Rao, R. P. N. & Ballard, D. H. Predictive coding in the visual cortex: a functional interpretation of some extra-classical receptive-field effects. *Nat Neurosci* **2**, 79–87 (1999).

15. Friston, K. A theory of cortical responses. *Phil. Trans. R. Soc. B* **360**, 815–836 (2005).

16. Keller, G. B. & Mrsic-Flogel, T. D. Predictive Processing: A Canonical Cortical Computation. *Neuron* **100**, 424–435 (2018).

17. Von Helmholtz, H. *Handbuch der physiologischen Optik*. (1867).

18. O'Toole, S. M., Oyibo, H. K. & Keller, G. B. Molecularly targetable cell types in mouse visual cortex have distinguishable prediction error responses. *Neuron* **111**, 2918-2928.e8 (2023).

19. Bastos, A. M. *et al.* Canonical Microcircuits for Predictive Coding. *Neuron* **76**, 695–711 (2012).

20. Sawtell, N. B. *et al.* NMDA Receptor-Dependent Ocular Dominance Plasticity in Adult Visual Cortex. *Neuron* **38**, 977–985 (2003).

21. Gerfen, C. R., Paletzki, R. & Heintz, N. GENSAT BAC Cre-Recombinase Driver Lines to Study the Functional Organization of Cerebral Cortical and Basal Ganglia Circuits. *Neuron* **80**, 1368–1383 (2013).

22. Deverman, B. E. *et al.* Cre-dependent selection yields AAV variants for widespread gene transfer to the adult brain. *Nat Biotechnol* **34**, 204–209 (2016).

23. Dumoulin, S. O. & Wandell, B. A. Population receptive field estimates in human visual cortex. *NeuroImage* **39**, 647–660 (2008).

24. Erisken, S. *et al.* Effects of Locomotion Extend throughout the Mouse Early Visual System. *Current Biology* **24**, 2899–2907 (2014).

25. Niell, C. M. & Stryker, M. P. Modulation of Visual Responses by Behavioral State in Mouse Visual Cortex. *Neuron* **65**, 472–479 (2010).

26. Kirchberger, L., Mukherjee, S., Self, M. W. & Roelfsema, P. R. Contextual drive of neuronal responses in mouse V1 in the absence of feedforward input. *Sci. Adv.* **9**, eadd2498 (2023).

27. Jordan, R. & Keller, G. B. Opposing Influence of Top-down and Bottom-up Input on Excitatory Layer 2/3 Neurons in Mouse Primary Visual Cortex. *Neuron* **108**, 1194-1206.e5 (2020).

28. Seignette, K. *et al.* Experience shapes chandelier cell function and structure in the visual cortex. *eLife* **12**, RP91153 (2024).

29. Keller, G. B. & Sterzer, P. Predictive Processing: A Circuit Approach to Psychosis. *Annu. Rev. Neurosci.* **47**, annurev-neuro-100223-121214 (2024).

30. Summerfield, C., Wyart, V., Johnen, V. M. & De Gardelle, V. Human Scalp Electroencephalography Reveals that Repetition Suppression Varies with Expectation. *Front. Hum. Neurosci.* **5**, (2011).

31. Kok, P., Jehee, J. F. M. & de Lange, F. P. Less Is More: Expectation Sharpens Representations in the Primary Visual Cortex. *Neuron* **75**, 265–270 (2012).

32. Kumar, S., Kaposvari, P. & Vogels, R. Encoding of Predictable and Unpredictable Stimuli by Inferior Temporal Cortical Neurons. *Journal of Cognitive Neuroscience* **29**, 1445–1454 (2017).

33. Meyer, T. & Olson, C. R. Statistical learning of visual transitions in monkey inferotemporal cortex. *Proc. Natl. Acad. Sci. U.S.A.* **108**, 19401–19406 (2011).

34. Todorovic, A. & De Lange, F. P. Repetition Suppression and Expectation Suppression Are Dissociable in Time in Early Auditory Evoked Fields. *J. Neurosci.* **32**, 13389–13395 (2012).

35. Wacongne, C. *et al.* Evidence for a hierarchy of predictions and prediction errors in human cortex. *Proc. Natl. Acad. Sci. U.S.A.* **108**, 20754–20759 (2011).

36. Furutachi, S., Franklin, A. D., Mrsic-Flogel, T. D. & Hofer, S. B. *Cooperative Thalamocortical Circuit Mechanism for Sensory Prediction Errors*. http://biorxiv.org/lookup/doi/10.1101/2023.07.12.548664 (2023) doi:10.1101/2023.07.12.548664.

37. Richter, D., Kietzmann, T. C. & De Lange, F. P. *High-Level Prediction Errors in Low-Level Visual Cortex*. http://biorxiv.org/lookup/doi/10.1101/2023.08.21.554095 (2023) doi:10.1101/2023.08.21.554095.

38. Kirchberger, L. *et al.* The essential role of recurrent processing for figure-ground perception in mice. *Sci. Adv.* **7**, eabe1833 (2021).

39. Keller, A. J., Roth, M. M. & Scanziani, M. Feedback generates a second receptive field in neurons of the visual cortex. *Nature* **582**, 545–549 (2020).

40. Heindorf, M. & Keller, G. B. *Antipsychotic Drugs Selectively Decorrelate Long-Range Interactions in Deep Cortical Layers*. https://elifesciences.org/reviewed-preprints/86805v2 (2023) doi:10.7554/eLife.86805.2.

41. Garrett, M. *et al. Stimulus Novelty Uncovers Coding Diversity in Visual Cortical Circuits*. http://biorxiv.org/lookup/doi/10.1101/2023.02.14.528085 (2023) doi:10.1101/2023.02.14.528085.

42. Homann, J., Koay, S. A., Chen, K. S., Tank, D. W. & Berry, M. J. Novel stimuli evoke excess activity in the mouse primary visual cortex. *Proc. Natl. Acad. Sci. U.S.A.* **119**, e2108882119 (2022).

43. Schulz, A., Miehl, C., Berry, M. J. & Gjorgjieva, J. The generation of cortical novelty responses through inhibitory plasticity. *eLife* **10**, e65309 (2021).

44. Mumford, D. On the computational architecture of the neocortex. (1992).

45. Marvan, T., Polák, M., Bachmann, T. & Phillips, W. A. Apical amplification—a cellular mechanism of conscious perception? *Neuroscience of Consciousness* **2021**, niab036 (2021).

46. Marvan, T. & Phillips, W. A. Cellular mechanisms of cooperative context-sensitive predictive inference. *Current Research in Neurobiology* **6**, 100129 (2024).

47. De Lange, F. P., Heilbron, M. & Kok, P. How Do Expectations Shape Perception? *Trends in Cognitive Sciences* **22**, 764–779 (2018).

48. Richter, D., Heilbron, M. & De Lange, F. P. Dampened sensory representations for expected input across the ventral visual stream. *Oxford Open Neuroscience* **1**, kvac013 (2022).

49. Blank, H. & Davis, M. H. Prediction Errors but Not Sharpened Signals Simulate Multivoxel fMRI Patterns during Speech Perception. *PLoS Biol* **14**, e1002577 (2016).

50. Han, B., Mostert, P. & De Lange, F. P. Predictable tones elicit stimulus-specific suppression of evoked activity in auditory cortex. *NeuroImage* **200**, 242–249 (2019).

51. Grill-Spector, K., Henson, R. & Martin, A. Repetition and the brain: neural models of stimulus-specific effects. *Trends in Cognitive Sciences* **10**, 14–23 (2006).

52. Pak, A., Ryu, E., Li, C. & Chubykin, A. A. Top-Down Feedback Controls the Cortical Representation of Illusory Contours in Mouse Primary Visual Cortex. *J. Neurosci.* **40**, 648–660 (2020).

53. Thiele, A. & Bellgrove, M. A. Neuromodulation of Attention. *Neuron* **97**, 769–785 (2018).

54. Disney, A. A., Aoki, C. & Hawken, M. J. Gain Modulation by Nicotine in Macaque V1. *Neuron* **56**, 701–713 (2007).

55. Pinto, L. *et al.* Fast modulation of visual perception by basal forebrain cholinergic neurons. *Nat Neurosci* **16**, 1857–1863 (2013).

56. Herrero, J. L. *et al.* Acetylcholine contributes through muscarinic receptors to attentional modulation in V1. *Nature* **454**, 1110–1114 (2008).

57. Williams, S. R. & Fletcher, L. N. A Dendritic Substrate for the Cholinergic Control of Neocortical Output Neurons. *Neuron* **101**, 486-499.e4 (2019).

58. Sridharan, D. & Knudsen, E. I. Selective disinhibition: A unified neural mechanism for predictive and post hoc attentional selection. *Vision Research* **116**, 194–209 (2015).

59. Zhang, S. *et al.* Long-range and local circuits for top-down modulation of visual cortex processing. *Science* **345**, 660–665 (2014).

60. Myers-Joseph, D., Wilmes, K. A., Fernandez-Otero, M., Clopath, C. & Khan, A. G. Disinhibition by VIP interneurons is orthogonal to cross-modal attentional modulation in primary visual cortex. *Neuron* **112**, 628-645.e7 (2024).

61. Talluri, B. C. *et al.* Activity in primate visual cortex is minimally driven by spontaneous movements. *Nat Neurosci* **26**, 1953–1959 (2023).

62. Van Beest, E. H. *et al.* Mouse visual cortex contains a region of enhanced spatial resolution. *Nat Commun* **12**, 4029 (2021).

63. De Kraker, L. *et al.* SpecSeg is a versatile toolbox that segments neurons and neurites in chronic calcium imaging datasets based on low-frequency cross-spectral power. *Cell Reports Methods* **2**, 100299 (2022).

64. Pnevmatikakis, E. A. & Giovannucci, A. NoRMCorre: An online algorithm for piecewise rigid motion correction of calcium imaging data. *Journal of Neuroscience Methods* **291**, 83–94 (2017).

65. Poort, J. *et al.* The Role of Attention in Figure-Ground Segregation in Areas V1 and V4 of the Visual Cortex. *Neuron* **75**, 143–156 (2012).

66. Knijnenburg, T. A., Wessels, L. F. A., Reinders, M. J. T. & Shmulevich, I. Fewer permutations, more accurate *P* -values. *Bioinformatics* **25**, i161–i168 (2009).

Key resource table

Reagent or resource	Source	Identifier
Virus		
AAV-PHP.eB-shortCAG-dlox-GCaMP6f(rev)-dlox	VVF Zurich	v657-PHP.eB
Mouse strains		
G35-3-Cre	Tonegawa lab (MIT)	MGI:4455188
TIT2L-GCaMP6f (Ai148D)	Jackson Laboratories	030328
Rbp4-Cre	GENSAT project	KL100

Statistical table

Figure	Comparison	Parameter	Test	# mice	N represents	# neurons	p-val	Sign
2E	Naive vs Expert	NO response	LMEM-Anova	6 vs 6	Neurons	884 vs 841	<0.001	***
	Naïve vs Task	NO response	LMEM-Anova	6 vs 6	Neurons	884 vs 300	<0.001	***
	Expert vs Task	NO response	LMEM-Anova	6 vs 6	Neurons	841 vs 300	0.9999	ns
	Naive vs Expert	O response	LMEM-Anova	6 vs 6	Neurons	884 vs 841	<0.001	***
	Naïve vs Task	O response	LMEM-Anova	6 vs 6	Neurons	884 vs 300	<0.001	***
	Expert vs Task	O response	LMEM-Anova	6 vs 6	Neurons	841 vs 300	<0.001	***
2J	Naive vs Expert	NO response	LMEM-Anova	5 vs 5	Neurons	497 vs 308	<0.001	***
	Naïve vs Task	NO response	LMEM-Anova	5 vs 5	Neurons	497 vs 422	<0.001	***
	Expert vs Task	NO response	LMEM-Anova	5 vs 5	Neurons	308 vs 422	0.0017	**
	Naive vs Expert	O response	LMEM-Anova	5 vs 5	Neurons	497 vs 308	0.8812	ns
	Naïve vs Task	O response	LMEM-Anova	5 vs 5	Neurons	497 vs 422	<0.001	***
	Expert vs Task	O response	LMEM-Anova	5 vs 5	Neurons	308 vs 422	<0.001	***
	L2/3 vs L5 effect (N vs E)	O response	LMEM-Anova	6 vs 5	Neurons	1725 vs 815	<0.001	***
3C	O vs O (naïve)	Correlation coef	Anova	6 vs 6	Mice	NA	<0.001	***
	NO vs NO (naïve)	Correlation coef	Anova	6 vs 6	Mice	NA	<0.001	***
	NO vs O (naïve)	Correlation coef	Anova	6 vs 6	Mice	NA	0.0007	**
	O vs O (expert)	Correlation coef	Anova	6 vs 6	Mice	NA	<0.001	***
	NO vs NO (expert)	Correlation coef	Anova	6 vs 6	Mice	NA	<0.001	***
	NO vs O (expert)	Correlation coef	Anova	6 vs 6	Mice	NA	0.0033	**
	O vs O (task)	Correlation coef	Anova	6 vs 6	Mice	NA	<0.001	***
	NO vs NO (task)	Correlation coef	Anova	6 vs 6	Mice	NA	<0.001	***
	NO vs O (task)	Correlation coef	Anova	6 vs 6	Mice	NA	0.0044	**
3D	NO vs O	Response onset	LMEM-Anova	6 vs 6	Neurons	584 vs 528	<0.001	***
3F	Naive vs Expert	NO selectivity	LMEM-Anova	6 vs 6	Neurons	884 vs 841	<0.001	***
	Naïve vs Task	NO selectivity	LMEM-Anova	6 vs 6	Neurons	884 vs 300	<0.001	***
	Expert vs Task	NO selectivity	LMEM-Anova	6 vs 6	Neurons	841 vs 300	0.845	ns
4C	O vs O (naïve)	Correlation coef	Anova	5 vs 5	Mice	NA	<0.001	***
	NO vs NO (naïve)	Correlation coef	Anova	5 vs 5	Mice	NA	<0.001	***
	NO vs O (naïve)	Correlation coef	Anova	5 vs 5	Mice	NA	0.3508	ns
	O vs O (expert)	Correlation coef	Anova	5 vs 5	Mice	NA	0.0013	**
	NO vs NO (expert)	Correlation coef	Anova	5 vs 5	Mice	NA	<0.001	***
	NO vs O (expert)	Correlation coef	Anova	5 vs 5	Mice	NA	0.2314	ns
	O vs O (task)	Correlation coef	Anova	5 vs 5	Mice	NA	<0.001	***
	NO vs NO (task)	Correlation coef	Anova	5 vs 5	Mice	NA	<0.001	***
	NO vs O (task)	Correlation coef	Anova	5 vs 5	Mice	NA	0.0565	ns
4D	NO vs O	Response onset	LMEM-Anova	5 vs 4	Neurons	584 vs 528	<0.001	***
4F	Naive vs Expert	NO selectivity	LMEM-Anova	5 vs 5	Neurons	497 vs 308	<0.001	***
	Naïve vs Task	NO selectivity	LMEM-Anova	5 vs 5	Neurons	497 vs 422	<0.001	***
	Expert vs Task	NO selectivity	LMEM-Anova	5 vs 5	Neurons	308 vs 422	0.0895	ns
5A	NO-NO vs chance	Decoding accuracy	Permutation test	6	Neurons	300	<0.001	***
	O-O vs chance	Decoding accuracy	Permutation test	6	Neurons	300	0.001	**
	NO-O vs chance	Decoding accuracy	Permutation test	6	Neurons	300	0.018	*
	O-NO vs chance	Decoding accuracy	Permutation test	6	Neurons	300	0.001	**
	NO-NO vs chance	Decoding accuracy	Permutation test	5	Neurons	422	<0.001	***
	O-O vs chance	Decoding accuracy	Permutation test	5	Neurons	422	<0.001	***
	NO-O vs chance	Decoding accuracy	Permutation test	5	Neurons	422	0.114	ns
	O-NO vs chance	Decoding accuracy	Permutation test	5	Neurons	422	0.032	*
5B	NO-NO vs chance	Decoding accuracy	Permutation test	175	Recording sites	NA	<0.001	***
	O-O vs chance	Decoding accuracy	Permutation test	175	Recording sites	NA	<0.001	***
	NO-O vs chance	Decoding accuracy	Permutation test	175	Recording sites	NA	0.007	**
	O-NO vs chance	Decoding accuracy	Permutation test	175	Recording sites	NA	<0.001	***
	NO-NO vs chance	Decoding accuracy	t-test	6	Humans	NA	<0.001	***
	O-O vs chance	Decoding accuracy	t-test	6	Humans	NA	0.0058	**
	NO-O vs chance	Decoding accuracy	t-test	6	Humans	NA	0.0081	**
	O-NO vs chance	Decoding accuracy	t-test	6	Humans	NA	0.0038	**

6C	Naive vs Expert	NO response	LMEM-Anova	6 vs 6	Neurons	884 vs 841	<0.001	***
	Naive vs Expert	O response	LMEM-Anova	6 vs 6	Neurons	884 vs 841	<0.001	***
6H	Naive vs Expert	NO response	LMEM-Anova	5 vs 5	Neurons	497 vs 308	<0.001	***
	Naive vs Expert	O response	LMEM-Anova	5 vs 5	Neurons	497 vs 308	0.4499	ns
S2A	Naive vs Expert	NO response	LMEM-Anova	6 vs 6	Neurons	884 vs 841	<0.001	***
	Naïve vs Task	NO response	LMEM-Anova	6 vs 6	Neurons	884 vs 300	<0.001	***
	Expert vs Task	NO response	LMEM-Anova	6 vs 6	Neurons	841 vs 300	0.9999	ns
	Naive vs Expert	O response	LMEM-Anova	6 vs 6	Neurons	884 vs 841	<0.001	***
	Naïve vs Task	O response	LMEM-Anova	6 vs 6	Neurons	884 vs 300	<0.001	***
	Expert vs Task	O response	LMEM-Anova	6 vs 6	Neurons	841 vs 300	<0.001	***
S2B	Naive vs Expert	NO response	LMEM-Anova	5 vs 5	Neurons	497 vs 308	<0.001	***
	Naïve vs Task	NO response	LMEM-Anova	5 vs 5	Neurons	497 vs 422	<0.001	***
	Expert vs Task	NO response	LMEM-Anova	5 vs 5	Neurons	308 vs 422	0.0116	*
	Naive vs Expert	O response	LMEM-Anova	5 vs 5	Neurons	497 vs 308	0.9999	ns
	Naïve vs Task	O response	LMEM-Anova	5 vs 5	Neurons	497 vs 422	<0.001	***
	Expert vs Task	O response	LMEM-Anova	5 vs 5	Neurons	308 vs 422	<0.001	***
S2C	Naive vs Expert	NO response	LMEM-Anova	6 vs 6	Neurons	884 vs 841	<0.001	***
	Naïve vs Task	NO response	LMEM-Anova	6 vs 6	Neurons	884 vs 300	0.0333	*
	Expert vs Task	NO response	LMEM-Anova	6 vs 6	Neurons	841 vs 300	0.2348	ns
	Naive vs Expert	O response	LMEM-Anova	6 vs 6	Neurons	884 vs 841	<0.001	***
	Naïve vs Task	O response	LMEM-Anova	6 vs 6	Neurons	884 vs 300	<0.001	***
	Expert vs Task	O response	LMEM-Anova	6 vs 6	Neurons	841 vs 300	<0.001	***
S2D	Naive vs Expert	NO response	LMEM-Anova	5 vs 5	Neurons	497 vs 308	0.0173	*
	Naïve vs Task	NO response	LMEM-Anova	5 vs 5	Neurons	497 vs 422	0.0161	*
	Expert vs Task	NO response	LMEM-Anova	5 vs 5	Neurons	308 vs 422	0.9999	ns
	Naive vs Expert	O response	LMEM-Anova	5 vs 5	Neurons	497 vs 308	0.2704	ns
	Naïve vs Task	O response	LMEM-Anova	5 vs 5	Neurons	497 vs 422	<0.001	***
	Expert vs Task	O response	LMEM-Anova	5 vs 5	Neurons	308 vs 422	0.0046	**
S7A	Plasticity vs Selec. L2/3		Correlation coef	6 vs 6	Neurons			
S7B	Plasticity vs Selec. L5		Correlation coef	5 vs 5	Neurons			
S8A	NO-NO vs chance (N)	Decoding accuracy	Permutation test	6	Neurons	841	<0.001	***
	NO-NO vs chance (E)	Decoding accuracy	Permutation test	6	Neurons	884	<0.001	***
	NO-NO vs chance (T)	Decoding accuracy	Permutation test	6	Neurons	300	<0.001	***
	O-O vs chance (N)	Decoding accuracy	Permutation test	6	Neurons	841	<0.001	***
	O-O vs chance (E)	Decoding accuracy	Permutation test	6	Neurons	884	<0.001	***
	O-O vs chance (T)	Decoding accuracy	Permutation test	6	Neurons	300	0.001	**
	NO-O vs chance (N)	Decoding accuracy	Permutation test	6	Neurons	841	0.235	ns
	NO-O vs chance (E)	Decoding accuracy	Permutation test	6	Neurons	884	0.023	*
	NO-O vs chance (T)	Decoding accuracy	Permutation test	6	Neurons	300	0.018	*
	O-NO vs chance (N)	Decoding accuracy	Permutation test	6	Neurons	841	0.070	ns
	O-NO vs chance (E)	Decoding accuracy	Permutation test	6	Neurons	884	0.029	*
	O-NO vs chance (T)	Decoding accuracy	Permutation test	6	Neurons	300	0.001	**
	NO-NO vs chance (N)	Decoding accuracy	Permutation test	5	Neurons	497	<0.001	***
	NO-NO vs chance (E)	Decoding accuracy	Permutation test	5	Neurons	308	<0.001	***
	NO-NO vs chance (T)	Decoding accuracy	Permutation test	5	Neurons	422	<0.001	***
	O-O vs chance (N)	Decoding accuracy	Permutation test	5	Neurons	497	0.020	*
	O-O vs chance (E)	Decoding accuracy	Permutation test	5	Neurons	308	<0.001	***
	O-O vs chance (T)	Decoding accuracy	Permutation test	5	Neurons	422	<0.001	***
	NO-O vs chance (N)	Decoding accuracy	Permutation test	5	Neurons	497	0.093	ns
	NO-O vs chance (E)	Decoding accuracy	Permutation test	5	Neurons	308	0.060	ns
	NO-O vs chance (T)	Decoding accuracy	Permutation test	5	Neurons	422	0.114	ns
	O-NO vs chance (N)	Decoding accuracy	Permutation test	5	Neurons	497	0.016	*
	O-NO vs chance (E)	Decoding accuracy	Permutation test	5	Neurons	308	0.039	*
	O-NO vs chance (T)	Decoding accuracy	Permutation test	5	Neurons	422	0.032	*

Author contributions

	KS	LdK	PP	LP	BH	JM	MS	ML	PR	LM	CL
Experimental design	X			X						X	X
Data collection	X										
Data analysis	X	X	X			X	X				
Technical assistance					X						
Interpretation	X		X			X			X	X	X
Writing	X										X
Review/editing	X	X		X		X	X	X	X	X	X
Conceptualization	X									X	X
Funding acquisition				X				X		X	X

Acknowledgements

We thank all members of the Levelt lab for discussion and support. We thank staff of the animal facility and mechatronics department at the Netherlands Institute for Neuroscience for technical support. We thank Chris van der Togt, Enny van Beest, Paul Neering, Maaike van der Aa, Marija Žuvela, Jessie Lof and Anda de Witte for help with experiments. We thank Fraser Smith for help with the human data. This project received funding from the European Union's Horizon 2020 Research and Innovation Program under grant agreement nos. 785907 (HBP SGA2, CL, PR, ML & LM) and 945539 (HBP SGA3, CL, PR, ML & LM), and from the Biotechnology and Biological Sciences Research Council (BBSRC) "Layer-specific cortical feedback (LM with LSP). The authors declare that they have no competing interests. All data needed to evaluate the conclusions in the paper are present in the paper and/or the Supplementary Materials.

Supplemental figures

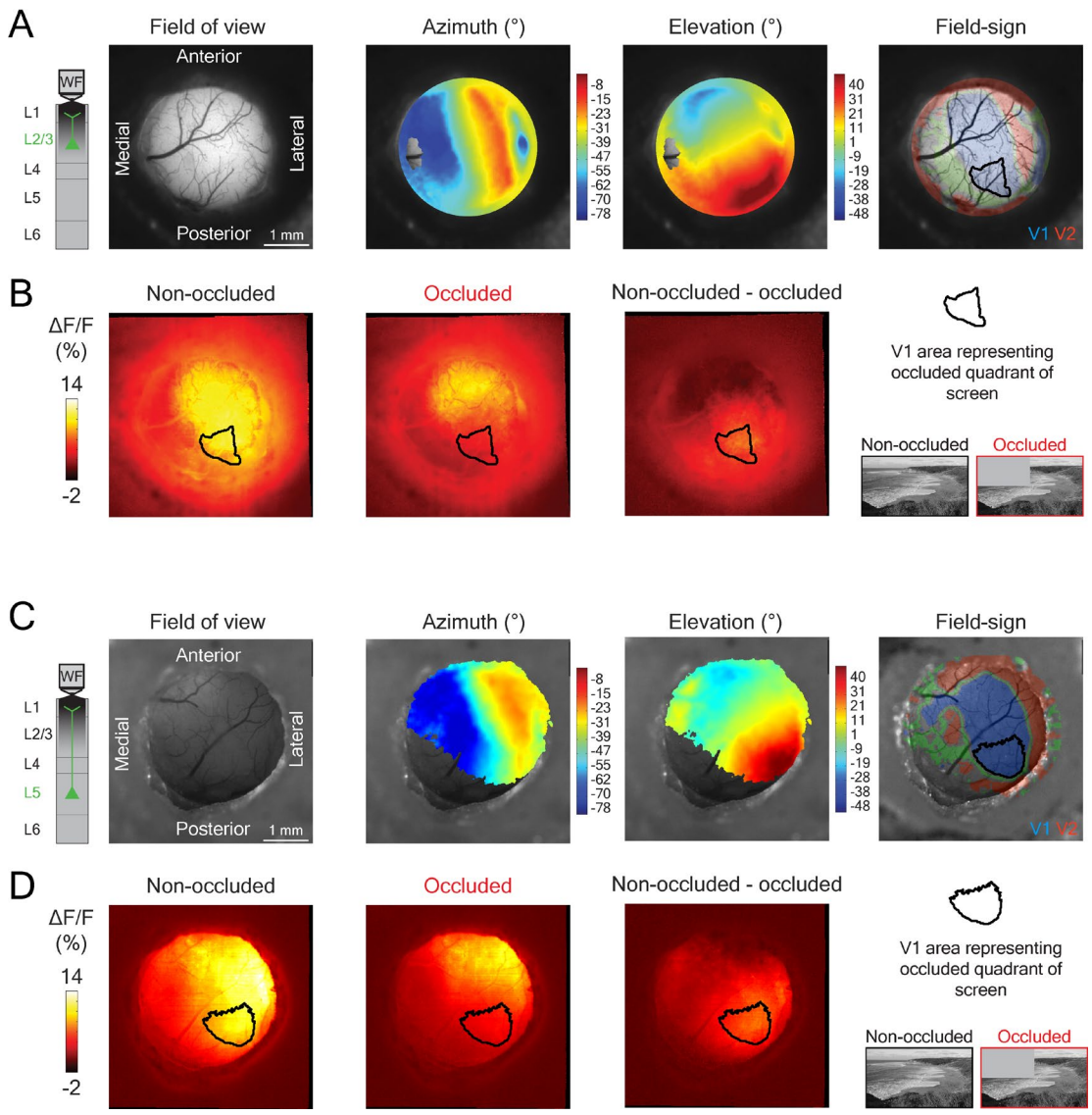

Figure S1. Mouse visual cortex responds to occluded images.

A) Cortical wide-field maps for an example L2/3 mouse showing from left to right: the imaging field of view, visual azimuth, visual elevation and visual field-sign overlaid on the brain imaged through the glass window. The large blue patch in the field-sign image represents V1 while the red patches represent higher visual areas (V2).
B) Cortical map showing average ΔF/F responses to the non-occluded and occluded stimuli for the example L2/3 mouse shown in A. The subtraction map shows a bright activity spot in the V1 area representing the occluded quadrant of the screen.
C) As in A, but for an example L5 mouse.
D) As in B, but for the example L5 mouse shown in C.

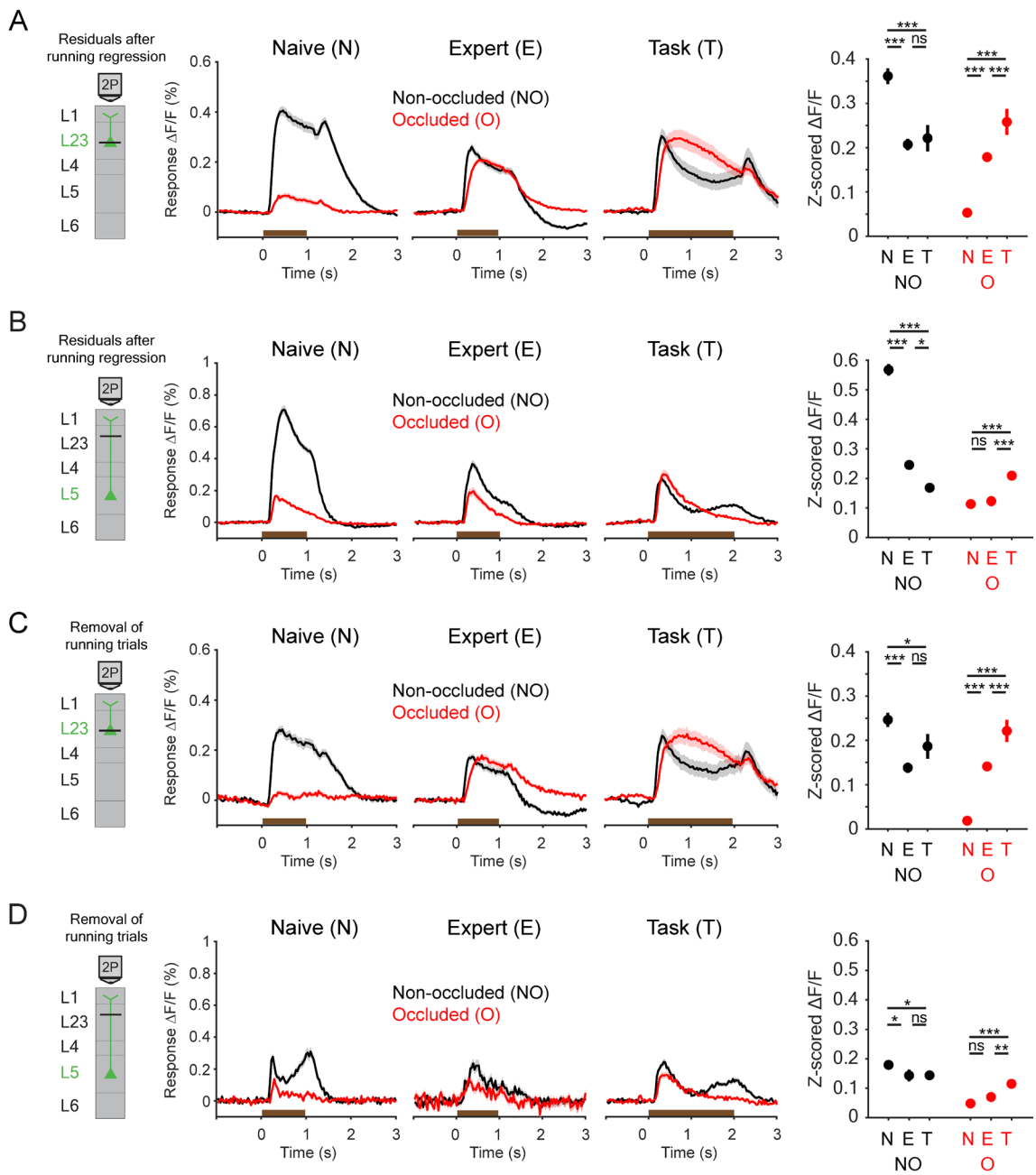

Figure S2. Locomotion does not explain experience-dependent plasticity.

A) Left: Schematic and z-scored ΔF/F traces averaged across L2/3 neurons and stimuli for all conditions after regressing out locomotion speed and performing analyses on the residual data. Brown bars indicate the presence of the visual stimulus. Right: neuron-averaged response strength across stimuli and conditions (mean ± SEM, averaged between t = 0.2-1 s) for L2/3 neurons after regressing out locomotion speed. N = 841 neurons (Naive), 844 neurons (Expert) and 300 neurons (Task) from 6 mice. LMEM with post hoc Tukey HSD for all comparisons here and below, ***: p<0.001, **: p<0.01, *: p<0.05, ns: not significant.

B) As in A, but for L5 neurons. N = 497 neurons (Naive), 308 neurons (Expert) and 422 neurons (Task) from 5 mice.

C) As in A, but for L2/3 data after removal of locomotion trials (average speed > 2 cm/s).

D) As in B, but for L5 data after removal of locomotion trials.

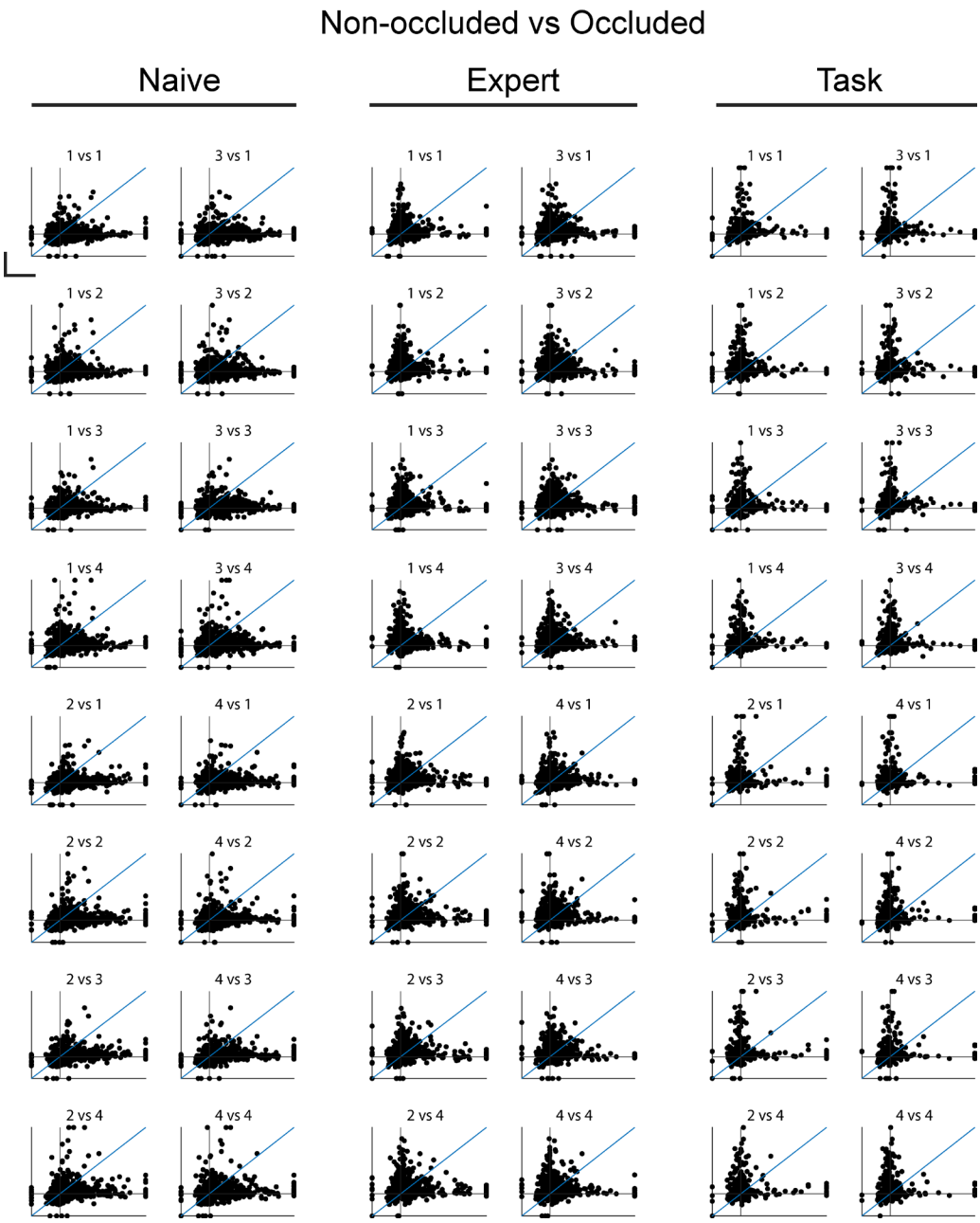

Figure S3. Relationship between responses to non-occluded and occluded images for L2/3 neurons.

Scatter plots showing the relationship between L2/3 responses to pairs of non-occluded and occluded images. Panel titles indicate the image comparisons made (non-occluded vs occluded). Axes are capped at -0.5 and 2.5 z-score. Scale bars, 1 z-scored ΔF/F.

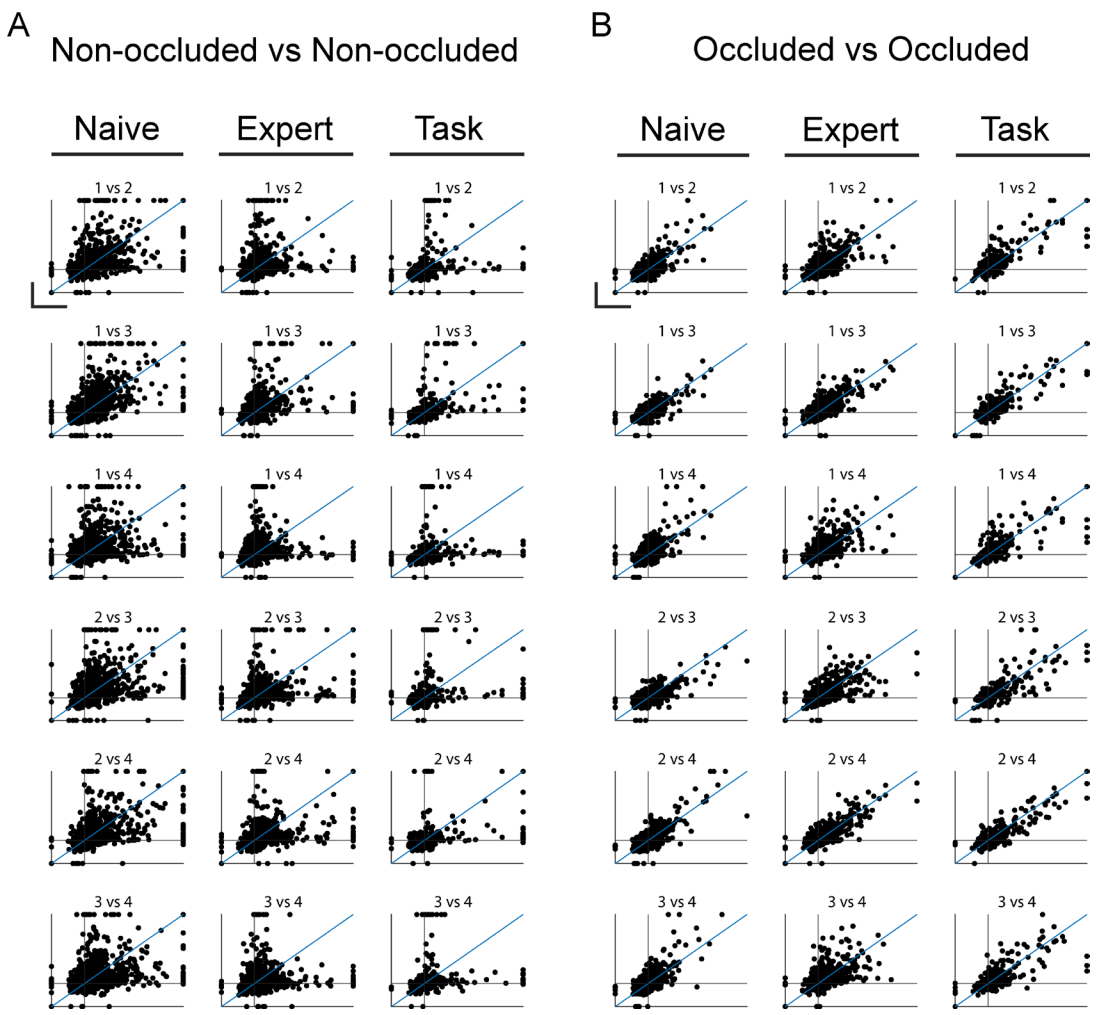

Figure S4. Relationship between responses to non-occluded and occluded images for L2/3 neurons.

A) Scatter plots showing the relationship between L2/3 responses to pairs of non-occluded images. Panel titles indicate the image comparisons made (non-occluded vs non-occluded). Axes are capped at -0.5 and 2.5 z-score. Scale bars, 1 z-scored ΔF/F.

B) As in A, but for pairs of occluded images.

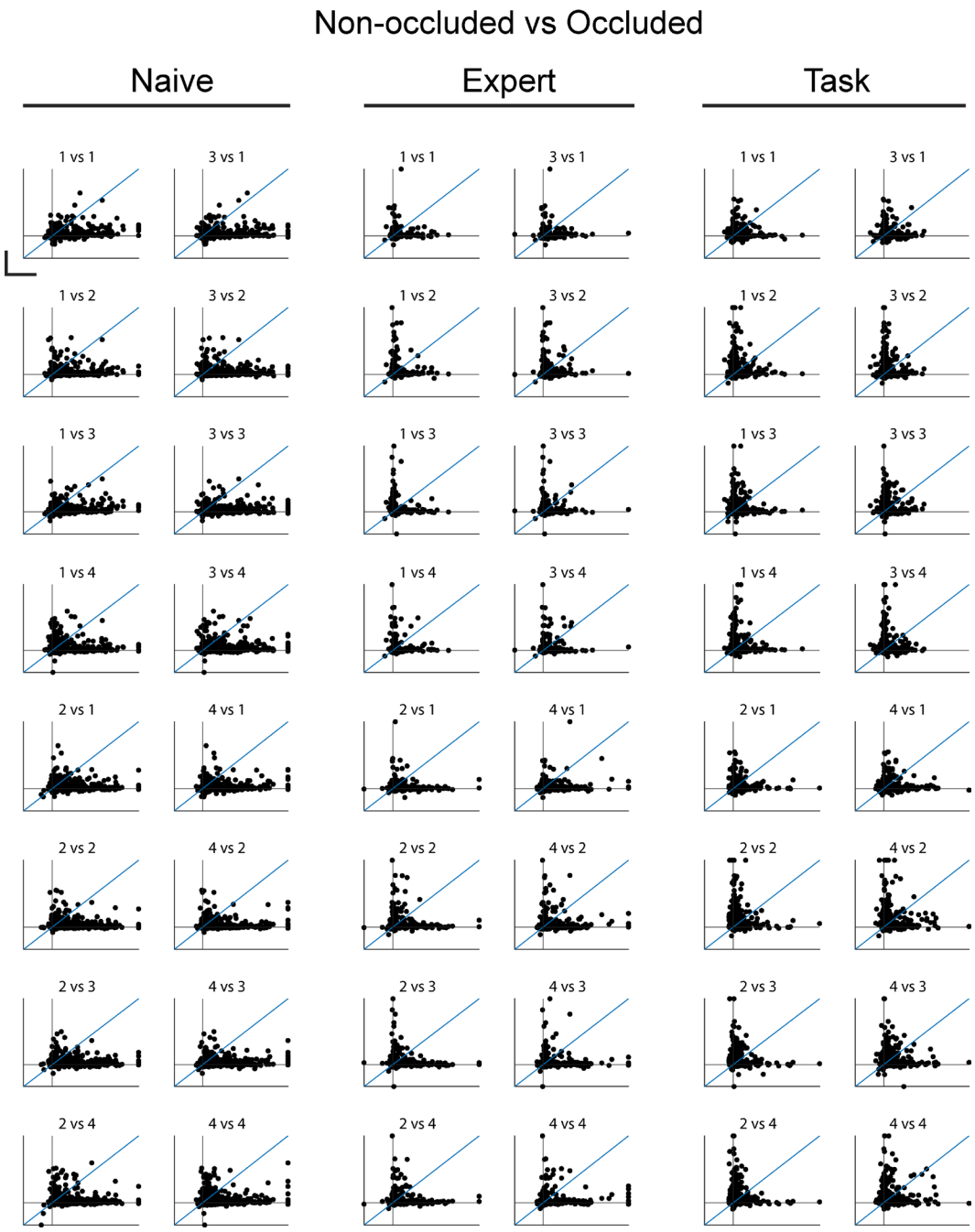

Figure S5. Relationship between responses to non-occluded and occluded images for L5 neurons.

Scatter plots showing the relationship between L5 responses to pairs of non-occluded and occluded images. Panel titles indicate the image comparisons made (non-occluded vs occluded). Axes are capped at -0.5 and 2.5 z-score. Scale bars, 1 z-scored ΔF/F.

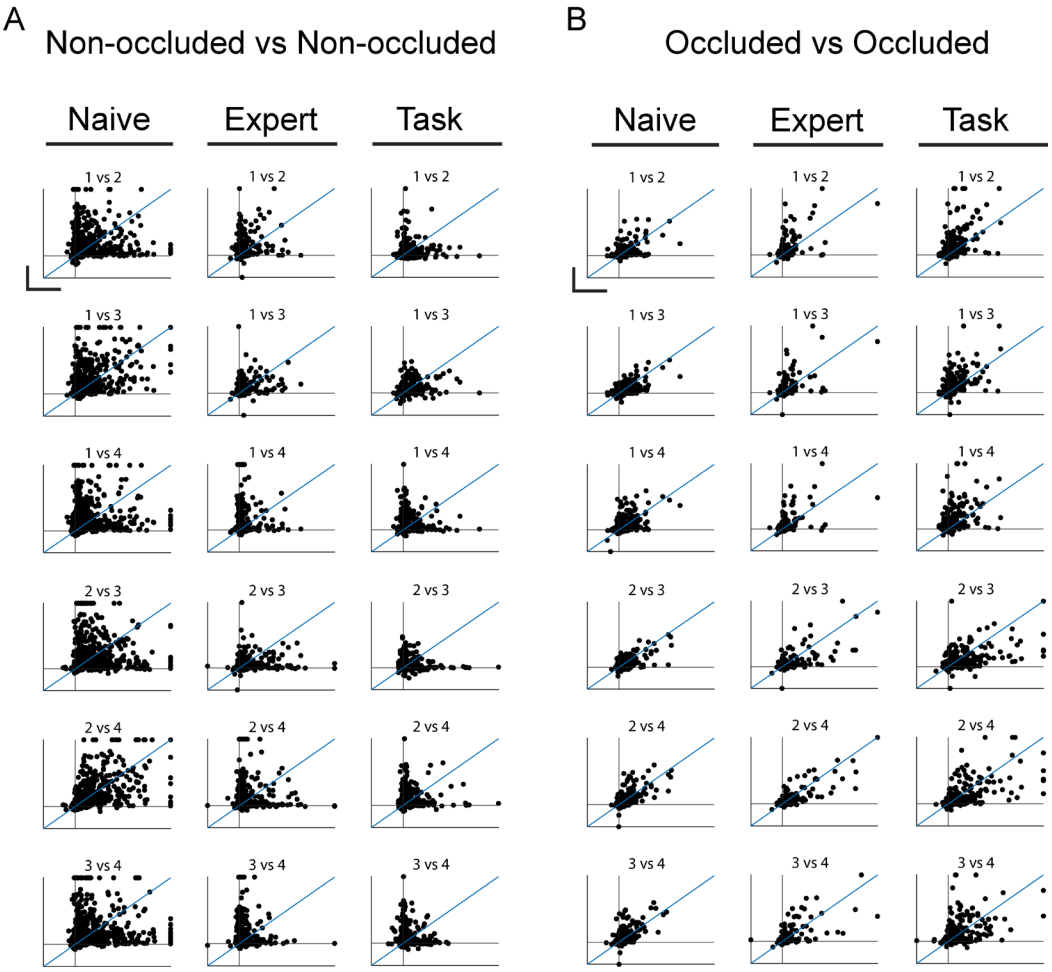

Figure S6. Relationship between responses to non-occluded and occluded images for L5 neurons.

A) Scatter plots showing the relationship between L5 responses to pairs of non-occluded images. Panel titles indicate the image comparisons made (non-occluded vs non-occluded). Axes are capped at -0.5 and 2.5 z-score. Scale bars, 1 z-scored ΔF/F.

B) As in A, but for pairs of occluded images.

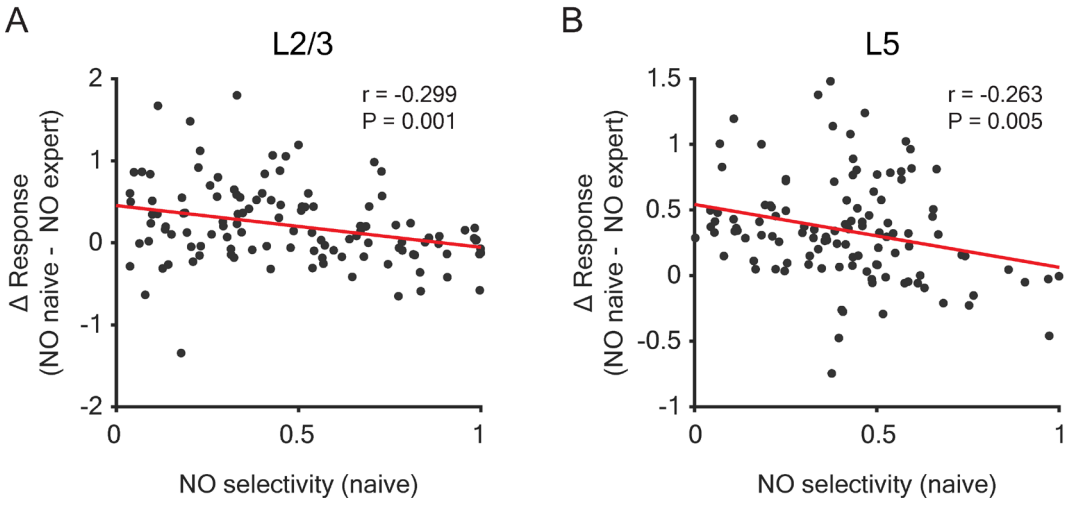

Figure S7. Relationship between non-occluded selectivity and plasticity.

A) Scatter plot showing the relationship between selectivity to non-occluded images and the change in response strength from Naive to Expert conditions in L2/3 neurons (n = 117 PyCs). NO, non-occluded.
B) As in A, but for L5 neurons (n = 114 PyCs).

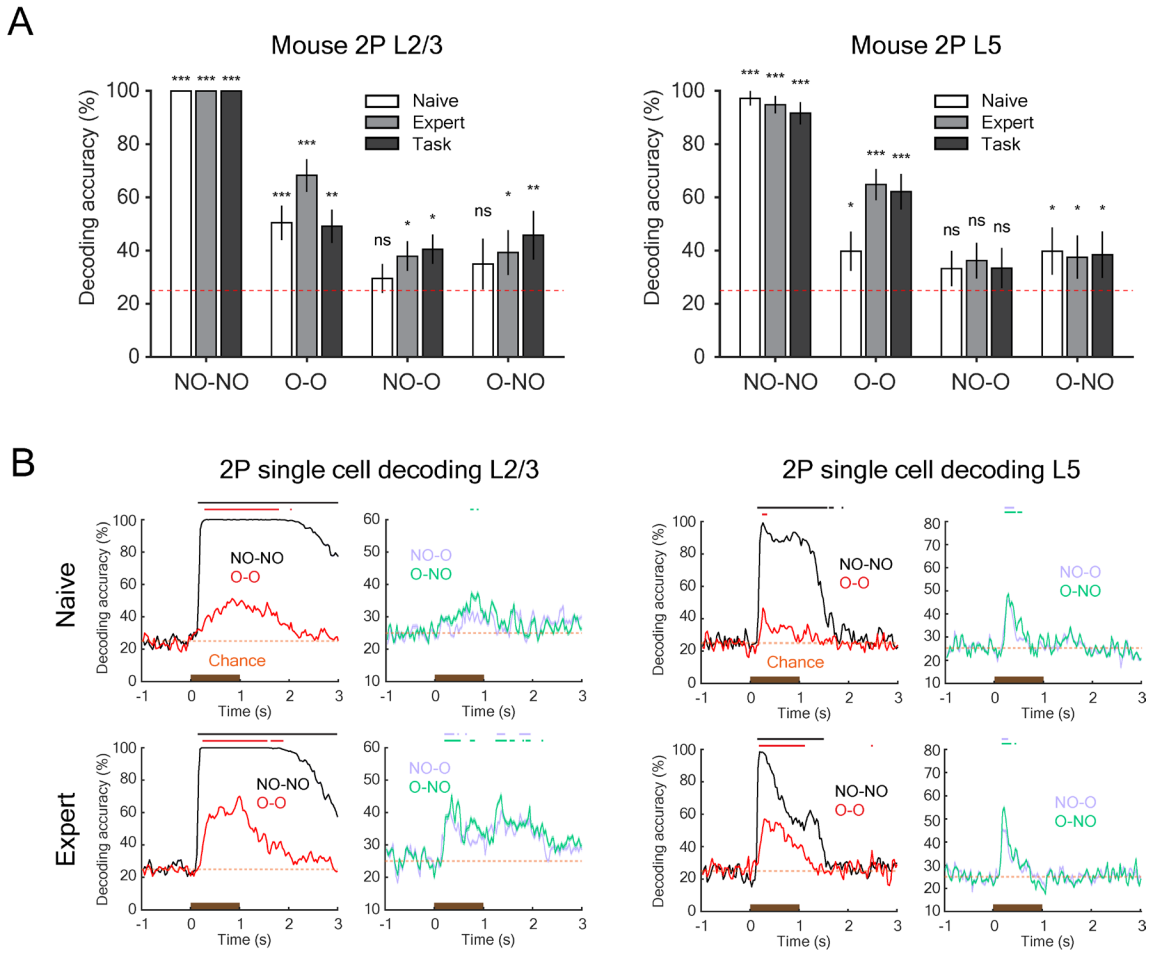

Figure S8. Decoding of visual and contextual signals across conditions.

A) Accuracy for population decoding of stimulus identity for mouse L2/3 neurons (left) and L5 neurons (right) across all conditions. We trained an LDA decoder on separate sets of trials for cross-validation (NO-NO, O-O) or cross-decoding (NO-O, O-NO). Bars show mean ± SEM across repetitions of decoding runs. Chance performance (orange dashed line) was 25%. N = 841 neurons (Naive), 844 neurons (Expert) and 300 neurons (Task) from 6 mice for L2/3 and N = 497 neurons (Naive), 308 neurons (Expert) and 422 neurons (Task) from 5 mice for L5. Permutation test, ***: p<0.001, **: p<0.01, *: p<0.05, ns: not significant. NO: non-occluded, O: occluded.

B) Population decoding accuracy over time for mouse L2/3 neurons (left) and L5 neurons (right). Colored dashes at the top depict significant time points (p<0.05, permutation test). Brown bars indicate the presence of the visual stimulus. Orange dashed line represents chance performance.